FINNISH METEOROLOGICAL INSTITUTE
CONTRIBUTIONS
No. 159

WAVES IN ARCHIPELAGOS

Jan-Victor Björkqvist

Institute for Atmospheric and Earth System Research
Faculty of Science
University of Helsinki
Helsinki, Finland

ACADEMIC DISSERTATION IN GEOPHYSICS

To be presented with the permission of the Faculty of Science of the University of Helsinki for public examination and criticism in auditorium E204 of the Physicum building (Gustaf Hällströmin katu 2, Helsinki) on the 10th of January, 2020, at 12 o'clock noon.

Finnish Meteorological Institute
Helsinki, 2020

Supervisor Dr Heidi Pettersson
Marine Research
Finnish Meteorological Institute
Helsinki
Finland

Pre-examiners Prof. Jaak Monbaliu
Department of Civil Engineering
Katholieke Universiteit Leuven
Leuven
Belgium

Prof. Alexander Babanin
Department of Infrastructure Engineering
University of Melbourne
Melbourne
Victoria
Australia

Opponent Dr Luigi Cavaleri
Institute of Marine Sciences (ISMAR) - National Research Council (CNR)
Venice
Italy

Custos Prof. Petteri Uotila
Institute for Atmospheric and Earth System Research
Faculty of Science
University of Helsinki
Helsinki
Finland

ISBN 978-952-336-092-1 (paperback)
ISSN 0782-6117
Edita Prima Oy
Helsinki 2020

ISBN 978-952-336-093-8 (pdf)
Helsinki 2020

ILMATIETEEN LAITOS
METEOROLOGISKA INSTITUTET
FINNISH METEOROLOGICAL INSTITUTE

Published by
Finnish Meteorological Institute
(Erik Palménin aukio 1), P.O. Box 503
FIN-00101 Helsinki, Finland

Series title, number and report code of publication
Finnish Meteorological Institute
Contributions 159, FMI-CONT-159

Date
January 2020

Author
Jan-Victor Björkqvist

Title
Waves in Archipelagos

Abstract

Waves are important for both the leisure and safety of the human population. Open-sea waves have been studied since the 1940's and their central properties are known. The wave field is described by the so called wave spectrum, which is a decomposition of the wave energy with respect to the wave frequency. In practice, the wave field is still often reduced to a few parameters, most importantly the dominant frequency (so called peak frequency) and the significant wave height. These parameters, however, does not sufficiently describe an archipelago wave field, but waves in archipelagos have still received relatively little attention from the scientific community. This thesis focuses on waves in archipelagos, and the study was carried out by using both numerical models and instrumental observations from the Helsinki archipelago and the Archipelago Sea in the Baltic Sea.

Waves in archipelagos are heavily affected by the numerous small islands; they attenuate long waves arriving from the open sea, while also defining new fetches for local waves. As a result, the wave spectrum has a wide frequency range where the energy is practically constant. The existence of this energy carrying range is in contrast to open sea measurements where the energy is concentrated around one dominant frequency. This study proposed a characteristic frequency that quantified the centre of the energy carrying range. For a traditional open sea spectrum the characteristic frequency closely resembled the dominant frequency, thus making it suitable for a wide range of wave conditions. The height of single waves in the archipelago were lower relative to the significant wave height. As a consequence, there was a large (10-15%) discrepancy between two definitions of the significant wave height; in the open sea this discrepancy is typically only 7-8%.

The three numerical models of this study simulated the archipelago wave field well. The largest discrepancy with the observations was found in an area just outside the archipelago that was sheltered by a peninsula. Inside the archipelago the models disagreed slightly on the energy distribution within the energy carrying range. These small differences strongly affected the dominant frequency in a way that was not representative of the good model performance. The differences were inconsequential for the significant wave height. During certain conditions the energy of the shortest waves were underestimated when using more advanced methods to calculate the energy transfer from the wind to the waves, most probably because a too small friction velocity. A simple older method to determine the friction velocity reproduced the shorter waves well. Coarse operational wind products were sufficient to force the high-resolution coastal wave models. Providing wind data only every third hour reduced the variability in the modelled wave field in the time scales between 2 and 10 hours. An hourly wind product captured all variations well, except for the statistical sampling variability in the measurements.

Spatial properties of the wave field were inferred from high-frequency wave staff measurements taken by R/V *Aranda*. These measurements were used to form a new wave spectrum where the waves are decomposed according to their inverse phase-speed. The new spectrum agreed well with the spatial wavenumber spectrum for the shortest waves, while the frequency spectrum did not. The good agreement between the inverse phase-speed spectrum and the wavenumber spectrum meant that the effect of the Doppler shift was small. The reason for the disparate results of the frequency domain were attributed to wave non-linearities. Using direct measurements to determining the waves as a function of their phase speed can be useful when studying the interaction between the wind and the waves, since no additional current measurements are needed to quantify the real wave speed relative to the wind.

Publishing unit
Finnish Meteorological Institute, Marine Research Unit

Classification (UDC)
551.46

Keywords
sea surface waves, archipelagos, wave modelling, wave measurements, Baltic Sea

ISSN and series title
0782-6117 Finnish Meteorological Institute Contributions

ISBN	Language	Pages
978-952-336-092-1 (paperback) 978-952-336-093-8 (pdf)	English	137

ILMATIETEEN LAITOS
METEOROLOGISKA INSTITUTET
FINNISH METEOROLOGICAL INSTITUTE

Utgivare
Meteorologiska institutet
(Erik Palméns plats 1)
PB 503, 00101 Helsingfors

Publikationens serie och nummer
Finnish Meteorological Institute
Contributions 159, FMI-CONT-159

Datum
Januari 2020

Författare
Jan-Victor Björkqvist

Rubrik
Skärgårdens vågor

Sammandrag

Havsvågor är viktiga för människor både ur ett rekreations- och säkerhetsperspektiv. Det öppna havets vågor har studerats sedan 1940-talet och deras centrala egenskaper är kända. Vågfältet beskrivs av det så kallade vågspektrumet, i vilket vågornas energi bryts med avseende på deras frekvens. I praktiken reduceras vågfältet ofta till några beskrivande parametrar, varav de viktigaste är den dominanta vågfrekvensen och den signifikanta våghöjden. Dessa parametrar beskriver inte vågorna i skärgården tillräckligt bra, men skärgårdens vågor har ändå fått tämligen lite vetenskaplig uppmärksamhet. Denna avhandling undersökte skärgårdens vågor både med numeriska modeller och observationer från Helsingfors skärgård och Skärgårdshavet.

Skärgårdens vågor påverkas i betydande grad av skärgårdens otaliga små öar; de dämpar längre vågor som anländer från det öppna havet, medan de samtidigt skapar nya svepsträckor för lokala vågor. Därför har vågspektrumet ett brett frekvensband där vågenergin är praktiskt taget konstant. Existensen av ett sådant här energibärande frekvensband står i kontrast till observationer från det öppna havet där energin är starkt koncentrerad kring en dominant frekvens. I detta arbete definierades en ny karakteristisk frekvens vilken beskriver medelpunkten av det energibärande frekvensbandet för skärgårdsvågor. För de typiska vågorna i öppna havet var denna nya karakteristiska frekvens nära den traditionella dominanta frekvensen, vilket gjorde denna nya parameter lämplig för att beskriva vågfält under vitt skilda omständigheter. I skärgården var höjden på de enskilda vågorna (i förhållande till den signifikanta våghöjden) lägre än på det öppna havet. Som en följd skilde sig de två traditionella definitionerna på den signifikanta våghöjden starkt (10-15%); på öppna havet är denna skillnad oftast bara 7-8%.

De tre numeriska vågmodellerna simulerade vågfältet i skärgården väl. De största felen fanns i ett område utanför skärgården som var delvis skyddat av Porkala udden. Inom skärgården betonade modellerna energidistributionen i det energibärande frekvensbandet på olika vis. För den traditionella dominanta frekvensen införde de små skillnaderna en stark avvikelse gentemot observationerna, även om denna avvikelse inte stod i proportion till de egentliga skillnaderna mellan modellerna och observationerna. För beräknandet av den signifikanta våghöjden var skillnaderna obetydliga. Under vissa omständigheter underbetonades energin för de korta vågorna ifall energiflödet från vinden till vågorna beräknades enligt en mera avancerad metod. Detta var troligen ett resultat av en för låg friktionshastighet. En äldre metod för att beräkna energiflödet till vågorna uppvisade inte en liknande avvikelse. De grova operativa vindprodukterna var tillräckliga för att driva vågmodellerna vid kusten, men modellerna kunde inte simulera vågfältets variationer med en tidsskala på 2–10 timmar ifall vindinformationen uppdaterades bara var tredje timme. Med vinddata som gavs varje timme kunde modellen fånga alla variationer, förutom den statistiska variabiliteten i vågobservationerna.

Genom att använda R/V *Arandas* högfrekventa vågobservationer tagna med kapacitiva trådar kunde även spatiell information deduceras. Dessa observationer användes för att definiera ett nytt vågspektrum i vilket vågorna beskrivs genom deras (inverterade) fashastighet istället för deras frekvens eller vågnummer (inversen av våglängden). Detta nya vågspektrum stämde överens med det rent spatiella vågnummerspektrumet för de kortaste vågorna, medan frekvensspektrumet gav olika resultat. Dopplereffekten bedömdes vara liten, eftersom den skulle ha påverkat fashastighetsspektrumet. Orsaken till skillnaderna var vågornas icke-linjära egenskaper, vilka påverkade den högfrekventa delen av frekvensspektrumet. Att beskriva vågorna med hjälp av den direkt observerade fashastigheten kan vara användbar då man undersöker interaktionen mellan vinden och vågorna, eftersom man då inte behöver skilda vattenströmningsmätningar för att bestämma vågornas verkliga hastighet i förhållande till vindhastigheten.

Publikationsenhet
Meteorologiska institutet, enheten för havsforskning

Klassificering (UDK)
551.46

Nyckelord
ytvågor, skärgård, vågmodellering, vågobservationer, Östersjön

ISSN ja och serietitel
0782-6117 Finnish Meteorological Institute Contributions

ISBN
978-952-336-092-1 (paperback) 978-952-336-093-8 (pdf)

Språk
engelska

Sidantal
137

Preface

I never much liked physics. Don't get me wrong, it was OK, but more in the sense that it proved the usefulness of the mathematics I was learning. Especially wave motion felt foreign: $\cos(kx-\omega t)$. I mean, these guys can't even get time running in the right direction. Luckily you didn't have to choose the subjects for the matriculate exam in advance back then; I pretended to prepare for the physics questions, but then still wrote mostly history and philosophy. In the University I majored in mathematics and—while the courses in particle physics never really felt right—got swept away by algebraic topology.

With a looming graduation I realised that I was not flushed with job options. I secured a grant from the University covering a part of my salary for certain intern positions. Armed with this discount tag I thought I'd have a shot at the summer positions at FMI. I wasn't thrilled. My one-course-dabble with atmospheric physics a few years back had not ended well. I was, nonetheless, called in for an interview to the Marine research unit. During that interview Prof. Jari Haapala (now head of the unit) said that they were "*more of the $F = m\vec{a}$ kind of guys*", which felt mildly reassuring.

Now, I won't keep you in suspense. I got the job. The work was intriguing, but my interest was really peaked when I realised that several mathematicians worked in the field. In one of our many discussions Prof. Kimmo Kahma (also a proud mathematician) told me that, by the time he got into waves, he had read even less physics than I had. "*You will be fine*", he told me, "*as long as you have a strong background in Fourier analysis"*. Well, I didn't. To be more exact: I had never done a single Fourier transform in my life. I wasted no time and enrolled in the first possible course at the University. It turned out, however, that I didn't really have the prerequisites, since they assumed that everyone knew a lot of functional analysis. So that was fun. I still managed, and followed up with an applied course, taught by Prof. Kahma himself. Shortly after that I enrolled as Dr. Heidi Pettersson's PhD student and everything, more or less, fell into place.

I have been lucky that several people have overseen my work, thus providing a wealth of opinions. I want to thank my supervisor Dr. Heidi Pettersson for her patience and guidance over the years, and Dr. Laura Tuomi for introducing me to the art of numerical wave modelling. I was also privileged to work under the guidance of Prof. Kimmo Kahma before he retired, thus giving me a chance to absorb some scraps of his decades of knowledge.

Thanks to Dr. Lauri Laakso for encouraging me to visit Miami, and to Prof. William Drennan for inviting me to RSMAS; I learned a great deal during my visits, especially from my talks with Dr. Nathan Laxague and Dr. Milan Curic. The hospitality of Dr. Victor Alari from the Tallinn University of Technology is also very appreciated. I also want to express my gratitude to Jaak Monbaliu and Alexander Babanin for taking the time to function as the pre-examiners of my thesis, and to Luigi Cavaleri for agreeing to be my opponent. Lastly, I would like to thank Professors Matti Leppäranta and Petteri Uotila, my co-authors, my family, and all my friends who have supported me during the years.

Jan-Victor Björkqvist
Helsinki, December 2019

Contents

List of publications

I Björkqvist, J.-V., Tuomi, L., Fortelius, C., Pettersson, H., Tikka, K., and Kahma, K. K., 2017. Improved estimates of nearshore wave conditions in the Gulf of Finland, *Journal of Marine Systems*, 171, pp. 43–53, DOI: 10.1016/j.jmarsys.2016.07.005.

II Björkqvist, J.-V., Vähä-Piikkiö, O., Alari. V., Kuznetsova, A., and Tuomi, L., 2019. WAM, SWAN and WAVEWATCH III in the Finnish archipelago – the effect of spectral performance on bulk wave parameters, *Journal of Operational Oceanography*, DOI: 10.1080/1755876X.2019.1633236

III Björkqvist, J.-V., Pettersson, H., and Kahma, K. K., 2019: The wave spectrum in archipelagos, *Ocean Science*, 15, pp. 1469–1487, DOI: 10.5194/os-15-1469-2019.

IV Björkqvist, J.-V., Pettersson, H., Drennan, W. M., and Kahma, K. K.: A New Inverse Phase Speed Spectrum of Nonlinear Gravity Wind Waves, *Journal of Geophysical Research: Oceans*, 124, pp. 6097–6119, DOI: 10.1029/2018JC014904

The authors contributions

The author is fully responsible for the summary. In Paper I the author did the wave model simulations, data analysis and a main part of the writing. In Paper II the author participated in the planning and execution of some of the field measurements, did the WAM model simulations, the data analysis, and the main part of the writing. In Paper III the author participated in the planning and execution of some of the field measurements, and is responsible for the data analysis and the main part of the writing. In Paper IV the author participated in the design and construction of the wave measurement device, and in the data collection during the field expedition with R/V *Aranda*. The author also processed the raw wave data, and did the data analysis and the major part of the writing.

1 Introduction

1.1 Why study waves?

Waves bring us joy and recreation, but they can also be a security concern for seafarers and coastal constructions (SPM, 1984; Kahma et al., 2016b; Leijala et al., 2018). In addition to their direct effects, wind generated sea surface waves play an intriguing part in several processes by interacting with both the air-sea boundary and the sea bottom. They serve as a medium for the wind that generates them to penetrate below the surface; unlike currents that move matter, the waves capture the energy of the wind and propagate it to sub-surface layers, either locally or at a distant, before finally reaching the shore.

The energy and momentum trapped in the wave motion (and lost through breaking) increase the sub-surface turbulence (Terray et al., 1996; Babanin and Haus, 2009), thus enhancing the vertical mixing of the upper layer (Qiao et al., 2004; Huang and Qiao, 2010). At the same time the waves also impact the lowest atmospheric layer, releasing some of their energy as an increased turbulence in the air, or even creating low-level jets (Högström et al., 2009; Semedo et al., 2009). The fluxes of momentum, heat, and greenhouse gases have also been proposed to be partially controlled by waves (Sahlée et al., 2012; Kahma et al., 2016a; Gutiérrez-Loza et al., 2018). Waves also deform and break sea ice, which can possibly result in an enhanced melting (Squire, 2007; Steele, 1992).

While waves don't transport matter directly, their orbital motions cumulatively move the water particles through the so called Stokes drift (Kenyon, 1969). This movement affects the drift of objects and the dispersion of materials at sea (Perrie et al., 2003; Tuomi et al., 2018) and is also a factor in the creation of Langmuir turbulence, which enhances the mixing of the surface layer (Langmuir, 1938; Belcher et al., 2012). When a wave breaks it also loses momentum to its surroundings, thus creating slopes in the water level that are eventually released into currents. This effect is particularly dominant at shallow surf zones where heavy wave breaking can take place (Longuet-Higgins, 1970), possibly leading to dangerous rip currents. Nearshore currents affect sediment transport and the living conditions of benthic animals, especially in combination with the near bottom orbital velocities of longer waves (Nielsen, 1988; Erm et al., 2011; Kaitaranta et al., 2013; Rinne et al., 2014).

Waves are an integral part of evolving weather patterns and ecosystems by linking otherwise disconnected events, not only in place, but also in time through the effects of swell. Conversely, how the waves develop are determined by their environment. Archipelagos—made up of a collection of small islands—have an irregular fetch geometry and complex bathymetrical conditions. Waves formed under such conditions are unique and deserve to be studied.

1.2 Describing the wave field

The wave spectrum contains the information of the sea state and describes how the energy of the wave field is distributed between different frequencies (ω) and directions (θ).

Parameters derived from the spectrum are a robust way to describe the central features of the wave field, with typical examples being the total energy and the dominant wave frequency. These variables, especially their growth with fetch, have been extensively studied (Toba, 1972; Hasselmann et al., 1973; Donelan et al., 1985; Kahma and Calkoen, 1992).

Waves shorter than the dominant wave frequency are typically described by a power law in spectral space. Different theoretical and dimensional arguments for ω^{-5} and ω^{-4} power laws have been presented, and both forms have experimental support (Phillips, 1958; Kitaigorodskii, 1962; Toba, 1973; Kahma, 1981; Kitaigorodskii, 1983; Phillips, 1985; Battjes et al., 1987; Banner, 1990). Consequently, spectral parameterizations and prognostic tails in wave models have assumed either an ω^{-4} or ω^{-5} structure (Hasselmann et al., 1973; Donelan et al., 1985; Komen et al., 1994; Booij et al., 1999). Yet, a body of research suggests that the rear face is made up of an wind-dependent ω^{-4} equilibrium range that transitions to a constant ω^{-5} saturation range for the highest frequencies. Significant efforts have been made to understand the energy levels of these two regions and the transition between them (e.g. Toba, 1973; Forristall, 1981; Kahma, 1981; Donelan et al., 1985; Resio and Perrie, 1989; Resio et al., 2004; Romero et al., 2010; Lenain and Melville, 2017).

1.3 Modelling the wave field

The possibility to describe the evolution of central wave parameters—combined with the existing parameterizations of the spectrum—led to the development of parametric wave prediction models (e.g. Hasselmann et al., 1976). There even existed a hope that the nonlinear wave interactions (Hasselmann, 1962) would force the wave spectra to a universal form. Nonetheless, later studies found that the connection between the peak frequency and the total energy varied with the fetch geometry, which consequently disproved the existence of a universal spectral shape (Holthuijsen, 1983; Kahma and Pettersson, 1994; Pettersson, 2004; Pettersson and Kahma, 2005).

Third-generation numerical wave models solve the action balance equation and predict the evolution of the wave spectrum without imposing any a priori restrictions on its shape. While originally developed for deep water (WAMDIG, 1988), models have also been adapted for coastal areas (Booij et al., 1999; Monbaliu et al., 2000). Examples of three popular models are WAM (WAMDIG, 1988; Komen et al., 1994), SWAN (Booij et al., 1999), and WAVEWATCH III® (WW3, Tolman et al., 2002). They are all based on the same principle, while differing in their numerical implementation and parameterization of the physical processes controlling wave evolution.

Special techniques have been implemented to account for islands smaller than the spatial resolution of the model (Tolman, 2003), and they have been proved to account for the attenuating effect of the islands well (Ponce de León and Guedes Soares, 2005, 2010). Numerical studies in water bodies with small islands have also been made, such as in the Baltic Sea (Tuomi et al., 2014), the Aegean Sea (Soukissian et al., 2004; Mazarakis et al., 2012), and Lake Superior (Anderson et al., 2015). Cavaleri et al. (2018), again, provided a thorough review of the state of modelling waves in coastal and inner seas, while also discussing the limitations of our current modelling approaches.

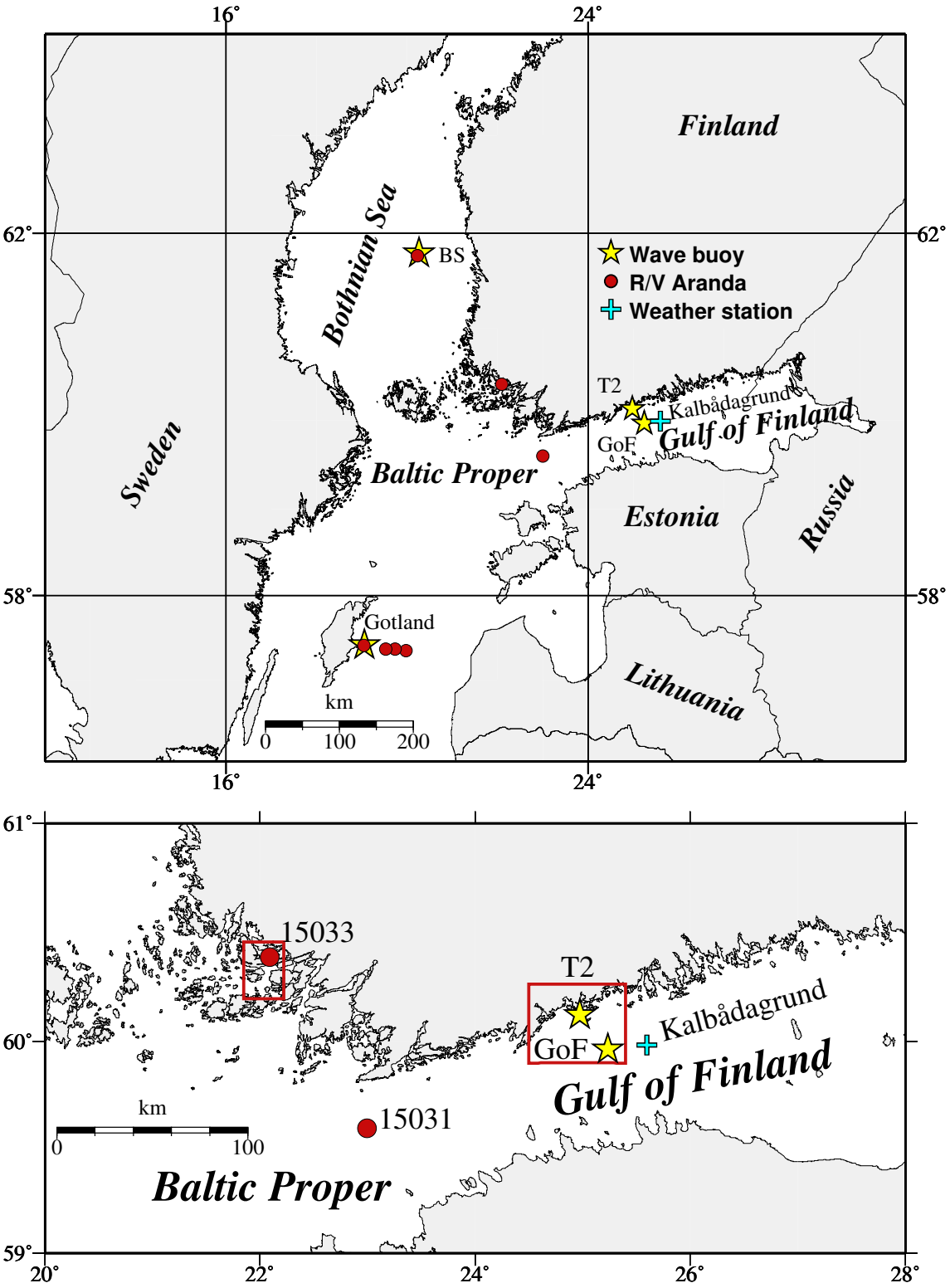

Figure 1.1: A map of the measurement locations in the Baltic Sea. The red boxes in the lower panel show the areas for the maps of the Archipelago Sea (Fig. 1.4) and the Helsinki archipelago (Fig. 1.3). Only permanent wave buoys are shown in this map. For an overview of all the wave measurements in the Helsinki archipelago, see Fig. 1.3. For the 15033 site, see Fig. 1.4.

Figure 1.2: A photograph of the Helsinki archipelago outside of Suomenlinna. (Photo: Jan-Victor Björkqvist)

1.4 Waves in the Baltic Sea

The Baltic Sea is a semi-enclosed basin with a longest fetch of about 700 km and a total area of 377,000 km^2. The wave climate in the Baltic Sea has been thoroughly mapped by both measurements and numerical wave hindcasts (Kahma et al., 2003; Jönsson et al., 2003; Cieślikiewicz and Paplińska-Swerpel, 2008; Räämet and Soomere, 2010; Tuomi et al., 2011; Pettersson et al., 2013; Björkqvist et al., 2018). The highest significant wave height of 8.2 m was measured in the Baltic Proper main basin (Tuomi et al., 2011). Nonetheless, the operational wave buoy in the Bothnian Sea sub-basin recently measured an 8.1 m significant wave height during the storm Aapeli in January 2019. A significant wave height over 9 m has been modelled both in the northern and southern part of the Baltic Proper (Tuomi et al., 2011; Björkqvist et al., 2018).

The Gulf of Finland (GoF) is a 60–120 km wide and 350 km long sub-basin of the Baltic Sea (Fig. 1.1). The narrowness of the gulf restricts wave growth and lines the wave directions along the basin (Kahma and Pettersson, 1994; Pettersson et al., 2010). Even though the dominant wind direction is from the south-west (Soomere and Keevallik, 2003), strong easterly winds are also possible. A 5.2 m significant wave height has been measured by the GoF wave buoy during strong winds from both east (Pettersson et al., 2013) and south-west (Tuomi et al., 2011).

Large parts of the Finnish coastline has a dense coastal archipelago. The main area of interest in this study was the Helsinki archipelago (Fig. 1.2), which is located on the southern Finnish coast in the GoF (Fig. 1.3). Measurements in the Helsinki archipelago have been conducted for coastal planning purposes (Kahma et al., 2016b), but they have seen limited scientific use. The other nearshore area studied in this thesis was the Archipelago Sea, which (together with the Åland Sea) separates the Baltic Proper from the Bothnian Sea (Fig. 1.1). It is only about 8,300 km^2 large, but still has over 40,000 islands. Very little wave measurements are available from the Archipelago Sea, but Tuomi et al. (2014) presented observations from a short campaign showing that the swell from the Baltic Proper was effectively attenuated by the islands and bottom processes. Wave mea-

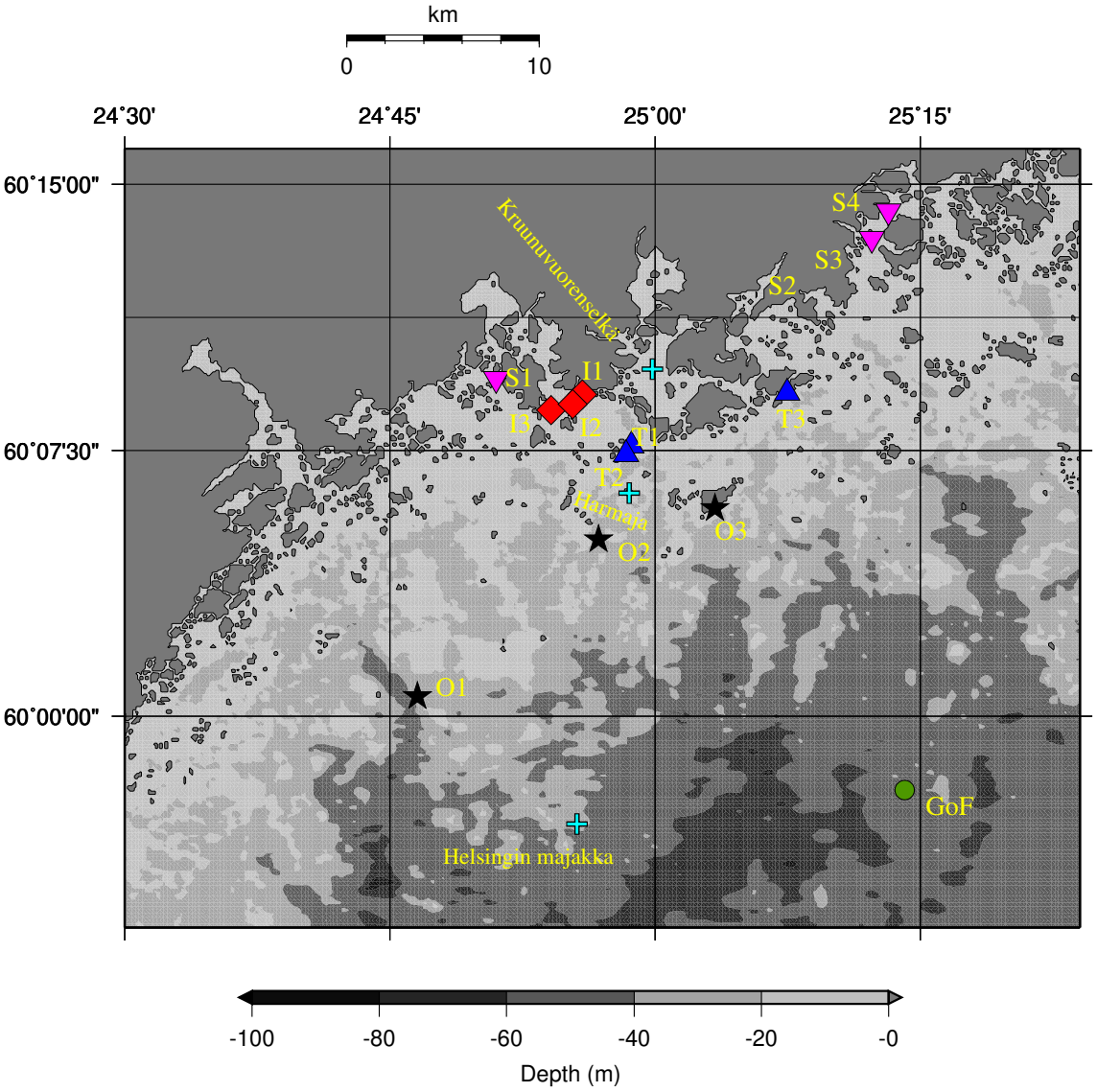

Figure 1.3: Measurement locations in the Helsinki archipelago. A plus (+) denotes wind measurements. The abbreviations are codes used for the wave buoy sites in Paper III, where O=Outer archipelago, T=Transition zone, I=Inner archipelago, and S=Sheltered archipelago. For the corresponding site names, see Table 3.1. The depth information is from the 0.1 nmi bathymetrical grid used in Paper I & II.

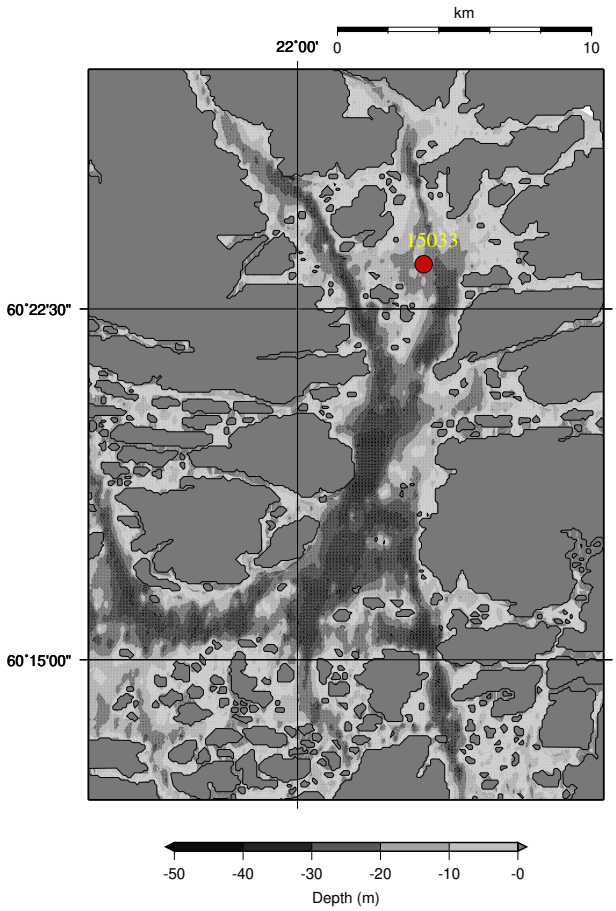

Figure 1.4: The measurement location in the Archipelago Sea where high-frequency measurements were available with several wave staffs. Measurement were taken with R/V *Aranda*.

surements from the Utö station at the southern edge of the Archipelago Sea exist (Tuomi and Björkqvist, 2014; Laakso et al., 2018), but this location is heavily exposed to waves propagating from the Baltic Proper.

1.5 Outline and aims of this study

Already Kahma (1979) presented wave measurements from the Bothnian Sea archipelago. Still, the characteristic features of waves in archipelagos have not yet been extensively studied, partly because of the relatively limited observational data. The main aim of this thesis was to fill this knowledge gap using in situ measurements and numerical models.

The properties of the waves inside the archipelago were compared with open sea measurements and results from previous studies. Special weight was given to the evolution of the wave spectrum through different parts of the archipelago (Paper II & III). In addition to quantifying the change in the spectral shape, the consequences for derived wave parameters, such as the significant wave height and the peak frequency, were also determined. The rear face of the spectrum was studied using high-frequency wave staff measurements (Paper IV). From these measurements, a new inverse phase-speed spectrum was defined,

and its properties were compared to the traditional frequency and wavenumber spectra.

Results from three numerical wave models were validated against extensive wave buoy measurements inside and outside the archipelago (Paper I & II). The abilities of the models to capture different features of the archipelago wave field were determined, as was the role of different forcing factors, such as the atmospheric and the bathymetrical data. The remaining challenges concerning archipelago implementations of the wave models, and the possible connection to the physical parameterization of the source terms, were discussed.

The main aims of this thesis were the following:

1. Identify how the wave spectrum changes when the waves propagate from the open sea towards the coast through the archipelago, and how the wave field in the archipelago compare with open sea wave conditions.

2. Determine how the atypical spectral shapes affect widely used wave parameters, such as the significant wave height and the peak frequency, and find suitable parameters to characterize the wave field in archipelagos.

3. Study how well state-of-the-art numerical wave models can reproduce the wave spectrum in the archipelago, how adequate the available wind forcings and bathymetrical data are for this task, and how the differences and shortcomings of the models are reflected in typical wave parameters and their validation.

4. Compare different numerical solutions and parameterizations of the physics, and identify topics where further study could lead to more accurate archipelago wave simulations.

5. Describe the rear face of the spectrum in different spectral domains, especially by using high-frequency measurements to define and study a new inverse phase-speed spectrum.

6. Study the power-law structures and their transitions are in all spectral domains, and use the inverse phase-speed spectrum to help explain the different results of the frequency spectrum and the wavenumber spectrum.

2 Definitions and mathematical methods

2.1 The wave spectrum

The investigation of sea surface waves starts with describing the water surface displacement at each time and location, denoted $\eta(x, y, t)$ (m). A Fourier transform of the autocorrelation function of $\eta(x, y, t)$ gives a frequency-wavenumber representation of the sea surface, called the wave spectrum. The full three-dimensional wave spectrum describes the variance density of the wave field as a function of the (angular) frequency, ω (rad s^{-1}), the wavenumber, k (rad m^{-1}), and the direction, θ (rad). This spectrum is denoted $\mathbb{F}(\omega, k, \theta)$ and normalized so that the total variance (m^2) of $\eta(x, y, t)$ is the integral

$$\mathrm{D}^2(\eta) = \iiint \mathbb{F}(\omega, k, \theta) k \; \mathrm{d}k\mathrm{d}\omega\mathrm{d}\theta. \tag{2.1}$$

Depending on the application and/or available data the spectrum is often given either as the wavenumber spectrum $\Psi(k, \theta)$ ($\mathrm{m}^4\mathrm{rad}^{-1}$), or as the frequency spectrum $\mathcal{S}(\omega, \theta)$ ($\mathrm{m}^2\mathrm{s\ rad}^{-1}$). These spectra follow by integration of Eq. 2.1 (over ω and k respectively). They can, however, also be determined directly from spatial or temporal data if only one or the other are available. The omnidirectional variants of these spectra are further obtained by integration:

$$F(k) = \int \Psi(k, \theta) k \; \mathrm{d}\theta \tag{2.2}$$

$$S(\omega) = \int \mathcal{S}(\omega, \theta) \; \mathrm{d}\theta. \tag{2.3}$$

If both the frequency and wavenumber of a single wave component is known, it is also possible to determine its phase-speed, since $c = \omega k^{-1}$ ($\mathrm{m\ s}^{-1}$). Previous studies have deduced spectral phase-speed information of e.g. transient eddies (Hayashi, 1982; Randel and Held, 1991). This work, however, also examined a representation of the wave field—formally defined for the first time in Paper IV—where the directional wave spectrum is given as a function of the inverse phase-velocity $\boldsymbol{\nu} = \mathbf{k}\omega^{-1}$ ($\mathrm{s\ m}^{-1}$), or the inverse phase-speed $\nu = |\boldsymbol{\nu}| = c^{-1}$. Also this spectrum was obtained by integration from the full spectrum:

$$\mathcal{Q}(\nu, \theta)\nu \, \mathrm{d}\nu = \int_{k/\omega=\nu} \mathbb{F}(\omega, k, \theta) k \; \mathrm{d}\omega\mathrm{d}k \tag{2.4}$$

$$\mathcal{Q}(\nu, \theta) = \frac{1}{\nu} \int \mathbb{F}(\omega, \omega\nu, \theta) \, \omega\nu \; \mathrm{d}\omega \left|\frac{\mathrm{d}k}{\mathrm{d}\nu}\right| \tag{2.5}$$

$$= \frac{1}{\nu} \int \mathbb{F}(\omega, \omega\nu, \theta) \, \omega^2\nu \; \mathrm{d}\omega \tag{2.6}$$

$$= \frac{1}{\nu} \int \mathbb{F}(k/\nu, k, \theta) \, \frac{k^2}{\nu^2} \; \mathrm{d}k, \tag{2.7}$$

where the last step simply switches the integrating variable from ω to k. This spectrum has the units $\mathrm{m^4 s^{-2} rad^{-1}}$, since the normalisation was chosen to resemble that of the wavenumber spectrum. Thus, the omnidirectional form ($\mathrm{m^3 s^{-1}}$) is given as (cf. Eq. 2.2):

$$Q(\nu) = \int \mathcal{Q}(\nu, \theta)\nu \, \mathrm{d}\theta. \tag{2.8}$$

The Jacobian $|\mathrm{d}k/\mathrm{d}\nu|$ was applied in Eq. 2.5 to give $Q(\nu)$ as variance density—not variance mass—with respect to ν, thus conserving the property of the integral being the variance of the wave field. Nevertheless, the definitions using integration were not applied in practice in this study, since observational data favours an approach where the variance was binned (see Sect. 2.1.2). Equations 2.4–2.7 are given here for completeness.

2.1.1 Fast Fourier Transform (FFT)

The omnidirectional frequency spectrum $S(\omega)$ is typically determined from a water level elevation time series at one point, i.e. $\eta(t)$. Assuming an ergodic process, the wave spectrum can be calculated from a single time series (e.g. Bendat and Piersol, 1986). The proper definition for the wave spectrum—as the power spectrum of $\eta(t)$—is the Fourier transform of the auto-covariance function of $\eta(t)$. Nevertheless, because of practical considerations, the spectrum is almost exclusively calculated using the Fourier transform of the original data, given here with the normalisation:

$$X(\omega_n) = \frac{1}{N} \sum_{j=0}^{N-1} \eta_j e^{-i2\pi nj/N}, \tag{2.9}$$

where $n \in \mathbb{N}$, N is the number of points in the observational time series, and η_j is the j:th data point. Typically, the Fourier transform is computed using the Fast Fourer Transform (FFT). The (singe sided) wave spectrum then follows as

$$S(\omega_n) = \frac{N\Delta t}{\pi} \langle |X(\omega_n)|^2 \rangle, \tag{2.10}$$

where $1 \leq n \leq N/2$ (assuming that N is even), Δt is the sampling time, $|\cdot|$ is the complex modulus, and $\langle \cdot \rangle$ is a general notation for the averaging that is required to achieve statistical stability. This stability is achieved by averaging elementary frequency bins, or by calculating the FFT from several blocks of the time series and averaging the results of these transforms. The latter technique was used by the Datawell wave buoys (Datawell, 2017), while the former was implemented to the wave staff data in Paper IV.

To avoid window leakage the original time series, η_j, were tapered with a window. The Datawell wave buoys used a Tukey window (Datawell, 2017), while a Blackman-Harris window was used for the wave staff data in Paper IV. The loss of variance caused by the window tapering was compensated in Eq. 2.10 to not violate the condition of Eq. 2.1.

2.1.2 Wavelet Directional Method (WDM)

The data from the multiple wave staffs (see Sect. 3.1.2) were analyzed using the Wavelet Directional Method (WDM, Donelan et al., 1996). The WDM gives information about the height $W(t, f)$ (m), as a function of time, t (s), and frequency (actually scale), f (Hz). This complex amplitude can be used to calculate the variance $|W(t, f)|^2$ (m^2). Using the phase lag between the different wave staffs the WDM determines the wavenumber $W_k(t, f)$ (rad m^{-1}) and the direction $W_\theta(t, f)$ (rad) of the waves. An exhaustive methodological description of the WDM is given in Donelan et al. (1996).

A number of different wavelets might be used. Following Donelan et al. (1996) and Tamura et al. (2014) we chose to use the Morlet wavelet (Grossmann and Morlet, 1984), which has a better frequency resolution compared to e.g. the Meyer wavelets (Meyer, 1989). The Morlet wavelets, however, are not orthogonal, thus leading to a loss of information for scales in between wavelets. This is compensated for by using intermediate wavelets (so called voices). Since voices are not independent, a large number of voices can give the illusion of a good frequency resolution, when in reality the neighboring frequencies are mostly dependent.

To convert the wavelet power, $|W(t, f)|^2$, to spectral density (m^2 Hz^{-1}s^{-1}) the proper normalization is given by

$$\mathbb{W}(t, f) = \frac{1}{\Delta t \Delta f} \frac{C_\mathrm{w}}{C_\mathrm{v}} |W(t, f)|^2, \tag{2.11}$$

where Δt and Δf is the time resolution and frequency resolution, C_v is the number of voices (including the base wavelet), and C_w is a factor accounting for the possible non-orthogonalities of the wavelets. For the orthogonal Meyer wavelets $C_\mathrm{w} = 1$ and for the Morlet wavelets used in this study $C_\mathrm{w} = 1.03565$.

Since the wavenumber modulus and the wave direction is known for each pair (f, t), an estimate for the wavenumber spectra, $F(k)$, was obtained by binning the variance $\mathbb{W}(t, f)\Delta t \Delta f$ with respect to the wavenumber modulus $W_k(t, f)$, and normalizing with the chosen bin width Δk. The directional wave spectra, $\mathcal{S}(\omega, \theta)$ and $\Psi(k, \theta)$, were determined by a similar binning technique with respect to both k and/or θ. Finally, the inverse phase-speed spectra, $Q(\nu)$ and $\mathcal{Q}(\nu, \theta)$ were calculated by binning the variance with respect to $\nu = k(2\pi f)^{-1}$ and/or θ. An overview of the chosen bin sizes etc. are found in the methods section of Paper IV.

2.1.3 Dimensionless quantities

Dimensionless quantities are a convenient way to describe physical processes. They allow us to compare experimental data from different conditions and establish possible universal properties. Dimensional analysis was adopted early to help study the wave spectrum, and the dimensionless quantities of the frequency and wavenumber spectra are established (Phillips, 1958; Kitaigorodskii, 1962). They are gathered in Table 2.1, along with the dimensionless quantities of the newly defined inverse phase-speed spectrum, which were determined in Paper IV.

Table 2.1: Dimensionless quantities Π_n of the different spectral representation. Also the forms of the ranges for rear face of the spectrum are given, where α is the saturation constant (Phillips, 1958) and α_u is the equilibrium constant (Kahma, 1981).

	$S(\omega)$ (m^2 s)	$F(k)$ (m^3)	$Q(\nu)$ (m^3 s^{-1})
Π_1	$\frac{S(\omega)\omega^4}{Ug}$	$\frac{F(k)k^{2.5}g^{0.5}}{U}$	$\frac{Q(\nu)\nu^4 g^2}{U}$
Π_2	$\frac{S(\omega)\omega^5}{g^2}$	$F(k)k^3$	$Q(\nu)\nu^5 g^2$
Π_3	$\frac{\omega U}{g}$	$\frac{kU^2}{g}$	$U\nu$
Equilibrium range	$\alpha_u U g \omega^{-4}$	$\frac{\alpha_u}{2} U g^{-0.5} k^{-2.5}$	$\alpha_u U g^{-2} \nu^{-4}$
Saturation range	$\alpha g^2 \omega^{-5}$	$\frac{\alpha}{2} k^{-3}$	$\alpha g^{-2} \nu^{-5}$

The dimensionless forms determine power law properties for certain parts of the wave spectrum. The rear face of the spectrum consists of an equilibrium range, followed by a saturation range. The equilibrium range scales with the wind speed, while the saturation range does not (Table 2.1). A schematic illustration of these ranges can be found in Fig. 2.1. If the water depth, h, is deep ($kh > \pi$), the ranges in the different spectral domains can be connected using linear theory, which is seen by the use of the same constants in all three domains. These dimensionless coefficients, α and α_u, are determined experimentally.

Phillips (1958) determined the constant α for the saturation range in the frequency domain. Following studies have calculated a value for α using both frequency and wavenumber measurement (e.g. Forristall, 1981; Leckler et al., 2015; Lenain and Melville, 2017). The equilibrium range constant was determined by Toba (1973) using laboratory data (and the friction velocity u_* instead of the wind speed U). Also the equilibrium range constant has been widely studied since (e.g. Forristall, 1981; Kahma, 1981; Donelan et al., 1985; Kahma, 1986; Resio et al., 2004). Both constants were determined for the inverse phase-speed spectrum based on the data of this study (Paper IV).

Although the equilibrium constant, α_u, have been considered universal, there is also evidence that it depends on the strength of the wind forcing (Donelan et al., 1985). The strength of the forcing wind is given relative to the phase speed of the spectral peak, U/c_p (also called the inverse wave age). This dependency can be accounted for by multiplying the equilibrium range with the dimensionless quantity $(U/c_p)^{p-1}$, following Donelan et al. (1985).

The exact transition between these two ranges has not yet been determined. Still, if the saturation range is assumed universal, the equilibrium level follows from the transition point (or vice versa). That is (in the frequency domain):

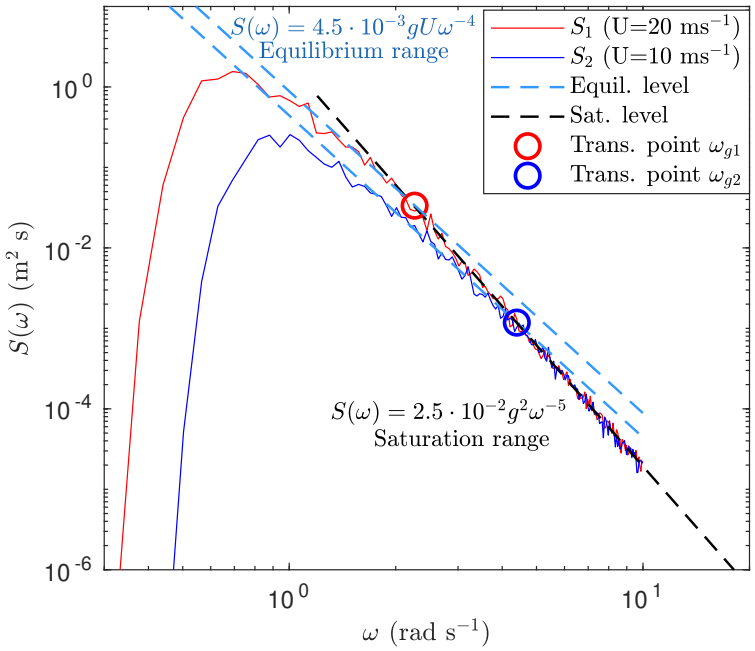

Figure 2.1: Schematic spectra showing the wind-dependent ω^{-4} equilibrium range and the transition to an ω^{-5} saturation range. The transition point $\omega_g U/g$ will be constant if the saturation level is fixed and the equilibrium level depend linearly on the wind speed.

$$\alpha_u \left(U/c_p\right)^{p-1} U g \omega_g^{-4} = \alpha g^2 \omega_g^{-5} \tag{2.12}$$

$$\frac{\omega_g U}{g} = \frac{\alpha}{\alpha_u}\left(\frac{U}{c_p}\right)^{1-p}, \tag{2.13}$$

where ω_g is the transition frequency, and g is the acceleration caused by gravity. Assuming deep-water linear theory, the phase speed is given by $c_p = g/\omega_p$, where ω_p is the peak frequency (Eq 2.19). For $p = 0$ the expression thus becomes $\omega_g/\omega_p = \alpha/\alpha_u =$ constant. In other words, the transition happens at a certain multiple of the peak frequency. This has been proposed by e.g. Banner (1990).

For $p = 1$ the term (U/c_p) vanishes, and the transition is determined by a constant dimensionless frequency: $\omega_g U/g = \alpha/\alpha_u$. This is consistent with Kahma (1981). Therefore, assuming a constant saturation range, the study of the equilibrium levels and transition points are just two sides of the same coin.

If deep water linear wave theory is assumed, the dimensionless transition frequency is the inverse wave age of the wave component with the frequency ω_g, since $\omega U/g = U/c$. Similarly, $kU^2/g = (U/c)^2$ in the wavenumber domain. In the inverse phase-speed domain no theoretical assumptions are needed, since $U\nu \equiv U/c$ by definition; this was the main motivations for defining the inverse phase-speed spectrum, $Q(\nu)$.

2.2 Wave parameters

2.2.1 Wave height

Many wave parameters are calculated using spectral moments, given as

$$m_n = \int \omega^n S(\omega)\,\mathrm{d}\omega. \tag{2.14}$$

The significant wave height, H_s, is calculated as

$$H_s = H_{m_0} = 4\sqrt{m_0}, \tag{2.15}$$

where $m_0 = \mathrm{D}^2(\eta)$ is the variance of the wave field. The notation H_{m_0} is used to distinguish Eq. 2.15 from the older definition, which is the mean height of the highest one-third of the individual waves in the time series. This parameter, $H_{1/3}$, is calculated by determining the individual wave height between two zero down-crossing and, after sorting them in descending order, calculating:

$$H_{1/3} = \frac{1}{N_\mathbf{w}/3} \sum_{i=1}^{N_\mathbf{w}/3} H_i, \tag{2.16}$$

where H_i is the height of a single wave and $N_\mathbf{w}$ is their total number.

The single highest wave of the time series is

$$H_{max} = \max\{H_i \,:\, 1 \leq i \leq N_\mathbf{w}\}, \tag{2.17}$$

while the maximum crest height is determined directly from the vertical displacement time series

$$\eta_{max} = \max\{\eta_j \,:\, 1 \leq j \leq N\}, \tag{2.18}$$

where N is the amount of data points.

2.2.2 Wave frequency

The definition of the peak frequency is the location of the spectral maximum, that is

$$\omega_p = \arg\max_\omega \, S(\omega). \tag{2.19}$$

In practise some smoothing method is often used when dealing with discrete spectra. All the papers in this study used a parabolic fit near the peak, but other methods also exist, such as that of Young (1995):

$$\omega_p^q = \frac{\int \omega S(\omega)^q \,\mathrm{d}\omega}{\int S(\omega)^q \,\mathrm{d}\omega}, \tag{2.20}$$

where q is a free parameter. Young (1995) proposed Eq. 2.20 with $q = 4$ as an alternative definition for the peak frequency. Although not an unbiased estimate for atypical wave conditions, Eq. 2.20 defines the "characteristic" frequency used in this study:

$$\omega_c = \omega_p^{q=4}. \tag{2.21}$$

The mean frequency is defined using the spectral moments as

$$\omega_m = \frac{m_1}{m_0}, \tag{2.22}$$

but is also obtained from 2.20 as $\omega_m = \omega_p^{q=1}$.

The wave periods follows from the wave frequency as

$$T_x = 2\pi \left(\omega_x\right)^{-1}, \tag{2.23}$$

where x refers to any of the frequency parameters ($x = p$ for ω_p etc.).

The spectral narrowness parameter by Battjes and van Vledder (1984) quantifies the narrowness (or peakedness) of the omnidirectional spectrum, and is defined as:

$$\kappa^2 = \frac{1}{{m_0}^2}\left(\left[\int_0^\infty S(\omega)\cos(\frac{\omega}{\omega_{m_{02}}})\,\mathrm{d}\omega\right]^2 + \left[\int_0^\infty S(\omega)\sin(\frac{\omega}{\omega_{m_{02}}})\,\mathrm{d}\omega\right]^2\right), \tag{2.24}$$

where $\omega_{m_{02}} = \sqrt{\frac{m_2}{m_0}}$. For an extremely narrow spectrum κ^2 tends to 1, while a wide spectrum has a κ^2 value close to 0.

3 The experimental set-up

3.1 Observational data

3.1.1 Wave buoy measurement

Most of the wave data in this study originated from Datawell Directional Waveriders. The larger (70–90 cm) buoys are equipped with accelerometers, and measure the accelerations, pitch, roll, and orientation of the device. They are all part of of FMI's operational fleet, but the Suomenlinna wave buoy (T2) is owned by the City of Helsinki. Additional measurements were made with smaller GPS-based DWR-G4 buoys. The majority of the G4-measurements were commissioned by the City of Helsinki (Kahma et al., 2016b), but some were also performed purely for research purposes. An overview of the measurement locations are given in Table 3.1, and a more detailed description of the data sets can be found in Papers I–IV.

3.1.2 Wave staff measurements

Wave staffs are submerged in the water and function as capacitors, with the capacitance changing with the water level. The omnidirectional wave spectrum can be calculated from the vertical water level displacements measured by a single wave staff. The thin wave staffs can measure shorter waves compared to wave buoys; wave staffs are a couple of mm thick, while wave buoys function as natural low-pass filters because of their size.

Directional and wavenumber spectra from the data taken with multiple wave staffs simultaneously were obtained using the WDM (Donelan et al., 1996, see also Sect. 2.1.2). The five wave staffs were installed in a fixed array that was submerged in front of a stationary R/V *Aranda*. The measurements were corrected for the movement of the ship following Drennan et al. (1994), and the motion correction and the calibration were validated against measurements from the Bothnian Sea wave buoy. A more detailed description of the experimental set-up is given in Paper IV.

3.1.3 Wind measurements

Wind data from the GoF were available from three FMI automatic weather stations (Fig. 1.3 Table 3.2). Paper II also used measurements from Kruunuvuorenselkä (Fig. 3.1), which have previously not been presented in any scientific paper.

Wind data was gathered by R/V *Aranda* simultaneously as the set-up measured the waves. Wind eddy covariance measurements were taken from the bow at the heights of 10.1 m and 16.2 m, of which the lower one was used since it was close to the 10 metre reference height.

A more detailed description of the wind measurements are found in the respective original articles.

Table 3.1: An overview of the wave measurement sites. R/V *Aranda* was a moving platform, while all other sites were fixed. The years refer to the years used in the study; data from the operational wave buoys of Gulf of Finland and Bothnian Sea are available for a longer time.

Station name	depth	Years	Device	Paper
Other				
R/V *Aranda* (15031–15044)	25–235 m	2015	Wave staffs	IV
Bothnian Sea (BS)	120 m	2015	DWR Mk-III	IV
Gulf of Finland (GoF)	62 m	2012–2018	DWR Mk-III / DWR4	I–III
Outer archipelago				
Harmaja (O1)	29 m	2012	DWR-G4	I–III
Isosaari (O2)	7 m	2014	DWR-G4	II, III
Berggrund (O3)	27 m	2015	DWR-G4	II, III
Transition Zone				
Länsikari (T1)	10 m	2013	DWR-G4	III
Suomenlinna (T2)	22 m	2016–2018	DWR Mk-III	II, III
Itä-Villinki (T3)	9 m	2013	DWR-G4	II, III
Inner archipelago				
Hernesaari (I1)	13 m	2012	DWR-G4	II, III
Ruumiskari (I2)	12 m	2014	DWR-G4	II, III
Jätkäsaari (I3)	13 m	2012	DWR-G4	II, III
Sheltered archipelago				
Koivusaari (S1)	5 m	2012	DWR-G4	III
Ramsinniemi (S2)	9 m	2013	DWR-G4	III
Vuosaaren satama (S3)	8 m	2013	DWR-G4	III
Talosaari (S4)	7 m	2013	DWR-G4	III

Table 3.2: Wind measurements platforms.

Station name	Height	Years	Eddy covariance	Paper
Kalbådagrund	32 m	2012–2016	No	I–III
Helsingin majakka	32 m	2012–2016	No	II
Harmaja	18 m	2012–2016	No	I–III
Kruunuvuorenselkä	13 m	2016	No	II
R/V *Aranda*	10 m	2015	Yes	IV

Figure 3.1: The wind measurements from inside the archipelago at Kruunuvuorenselkä (Fig. 1.3) (Photo: Jan-Victor Björkqvist).

3.2 Wave modelling

3.2.1 The principle of wave models

Phase averaged third-generation wave models are the state-of-the-art, and impose no a priori restrictions on the shape of the wave spectrum. These models solve the wave action balance equation, which in Cartesian coordinates can be written as:

$$\frac{\partial N}{\partial t} + \frac{\partial c_x N}{\partial x} + \frac{\partial c_y N}{\partial y} + \frac{\partial c_\sigma N}{\partial \sigma} + \frac{\partial c_\theta N}{\partial \theta} = \frac{G_{tot}}{\sigma}, \tag{3.1}$$

where $N(t, x, y; \sigma, \theta) = \mathcal{S}(t, x, y; \sigma, \theta)/\sigma$ is the wave action density, $\sigma = \omega - U_c k$ is the intrinsic frequency, U_c is the current speed, c_X is the propagation velocity of the wave variance with respect to different variables, t is the time, x, y are the Cartesian coordinates, and θ is the propagation direction. The reason for modelling the action density instead of the variance density is that the action density is conserved in the presence of currents, while the variance is not. In deep water without ambient currents the intrinsic frequency, σ, reduces to the frequency, ω. Eq. 3.1 can then be written in terms of the variance density, $\mathcal{S}(t, x, y; \omega, \theta)$.

The left side of Eq. 3.1 describes the propagation of wave variance and is solved numerically using an explicit or implicit solver. The explicit solvers of different order are subject to the CFL-condition. Implicit solvers are unconditionally stable, but require iteration to converge.

The right side term, G_{tot}, is the sum of source terms describing the change in wave variance that is caused by physical processes. In deep water the three processes considered

are the energy input by the wind (G_{in}), the dissipation of energy through whitecapping (G_{ds}), and the weakly non-linear four wave interactions (G_{nl}). The source terms accounting for finite depth effects are e.g.the bottom friction (G_{bot}), depth-induced wave breaking (G_{brk}), and non-linear three wave interactions (G_{nl3}).

3.2.2 WAM, SWAN, and WAVEWATCH III

Three numerical wave models were used in this study. WAM (WAMDIG, 1988; Komen et al., 1994; Monbaliu et al., 2000) was used in Papers I and II, while SWAN (Booij et al., 1999) and WAVEWATCH III® (WW3, Tolman et al., 2002) were used in Paper II. The models differ in their numerical scheme (used to solve the left side of Eq. 3.1) and their parameterization of the physical processes (right side of Eq. 3.1).

WAM is the oldest of the models and is built around a fixed set of source terms, as documented in Komen et al. (1994) and Bidlot et al. (2007). SWAN has a couple of options for the choice of deep water source terms, but the ones based on the work of Komen et al. (1984) and Komen et al. (1994) were chosen for this study. WW3 has the widest setting of source terms, but was implemented using the deep water source terms package of Ardhuin et al. (2010) (ST4). The weakly non-linear four wave interactions were calculated using the Discreet Interaction Approximation (DIA, Hasselmann et al., 1985) in all set-ups.

The depth-induced wave breaking formulation of Battjes and Janssen (1978) was used in all three models. The bottom friction was following Hasselmann et al. (1973) in WAM and SWAN, while the SHOWEX bottom friction (Ardhuin et al., 2003) was used in WW3. The non-linear three-wave interactions were only switched on in SWAN, using the Lumped Triad Approximation (LTA, Eldeberky, 1996).

WAM uses the explicit first order upwind scheme, while SWAN uses the implicit four sweep scheme. WW3 was run with the explicit third-order upwind scheme, since no implicit schemes were available for structured grids in v5.16 (although this possibility has been added in the newest version).

More exact descriptions of all the model settings are given in the first two original articles, but the details of the coastal implementations are also summarized in Table 3.3.

3.2.3 Bathymetric data

The nearshore model set-ups were implemented using a single nested grid covering the Helsinki archipelago (24° 28'–25° 24' E, 59° 52'–60° 16' N). The primary bathymetrical grid had a resolution of 0.1 nmi (185 m) and was mainly based on information from nautical charts (Björkqvist et al., 2014, Paper I). A second 0.1 nmi grid was also used in Paper I. This alternative grid was constructed within the *Velmu* project run by the Finnish Environmental Institute (http:// www.ymparisto.fi/en-US/VELMU/) using data from water quality stations and the Baltic Sea Bathymetric Database (BSBD, 2013).

The high-resolution grids were nested inside a 1 nmi (1.85 km) Baltic Sea grid. This coarser grid was based on ETOPO1 (Amante and Eakins, 2009) and data from IOW (Seifert et al., 2001) in Paper I. In Paper II it was based on Seifert et al. (2001) and

Table 3.3: Settings and physical parameterisations used in the wave models. All models were implemented with a 0.1 nmi structured grid nested inside a 1 nmi Baltic Sea grid.

Used in Paper	I, II	II	II
	WAM	SWAN	WW3
Model version	Cycle 4.5.1 (I), 4.5.4 (II)	41.10AB	v5.16
Advection time step	2 s	10 min, 5 iterations	5 s
Intra-spectral time step	N/A	N/A	2 s
Source term integration time step	2 s (I), 10 min (II)	10 min	10 min
Global time step	N/A	N/A	30 s
Propagation scheme	First order upwind	Fully implicit four sweep	Third order upwind
Wind input	Janssen (1991)	Komen et al. (1984); Wu (1982)	Ardhuin et al. (2010)
Dissipation	Komen et al. (1994): δ =0.5 (I), 0.6 (II)	Komen et al. (1994): $\delta = 1$	Ardhuin et al. (2010)
Bottom friction	Hasselmann et al. (1973)	Hasselmann et al. (1973)	SHOWEX (Ardhuin et al., 2003)
Wave breaking	Battjes and Janssen (1978)	Battjes and Janssen (1978)	Battjes and Janssen (1978)
Non-linear four wave	DIA (Hasselmann et al., 1985)	DIA (Hasselmann et al., 1985)	DIA (Hasselmann et al., 1985)
Non-linear triad	–	LTA (Eldeberky, 1996)	-

Table 3.4: The different numerical weather prediction systems used to force the wave models in this study.

Model name	Version	Resolution	Years	Operational data	Paper
HIRLAM	version 7.4	7.5 km* / 3 h	2012	Yes	I
HIRLAM	version 7.4	7.5 km / 1 h	2012–2015	Yes	II
HIRLAM	version 7.4	7.5 km / 3 h	2016	Yes	II
HARMONIE	cycle 38h1	1 km / 15 min	2012	No	I
HARMONIE	cycle 38h1.2	2.5 km / 1 h	2016	No	II

* Given to the wave model at a 11 km resolution.

the Baltic Sea Bathymetric Database (BSBD, 2013).

3.2.4 Wind forcing

Two different Numerical weather prediction (NWP) systems—HIRLAM and HARMONIE (HIRLAM-B, 2018)—were used to force the wave models runs (Table 3.4). The HIRLAM data originated from FMI's operational weather forecasts, while the HARMONIE hindcasts were made specifically for this study. The HIRLAM data given to the models was coarse compared to the wave model resolution (7.4–11 km vs 0.185 km) and HARMONIE was therefore implemented as an alternative forcing with a resolution of 1–2.5 km. The wind data were available with a time interval between 15 min and 3 hours. An overview of the NWP's are given in Table 3.4 and in the methods sections of Papers I and II.

4 The observed archipelago wave field

4.1 The wave spectrum

A schematic figure of an archipelago-type spectrum is presented in Fig. 4.1. The wide frequency range with constant energy, between roughly 1 and 2 rad s^{-1}, will henceforth be called the energy carrying range. Since the frequency bins in a measured wave spectrum are χ^2 distributed (e.g. Bendat and Piersol, 1986), it was possible to simulate random samples from this underlying, idealised, spectrum. These samples showed that the spectral peak was random within the energy carrying range—something already found in Paper II. The third "measured" sample (red) might also mistakenly be interpreted to signify a multimodal sea state, even though we know that the underlying spectrum showed no such characteristics.

Paper III found a systematic transition of the mean spectral shape in the Helsinki archipelago. In the open sea the mean spectrum was unimodal, while the flat spectrum in the archipelago was dominated by a wide energy carrying range (Fig. 2 in Paper III). The spectral shape was quantified by the κ^2 narrowness parameter (Eq. 2.24), which was smaller where the mean spectrum was visibly wider (Table 2 in Paper III).

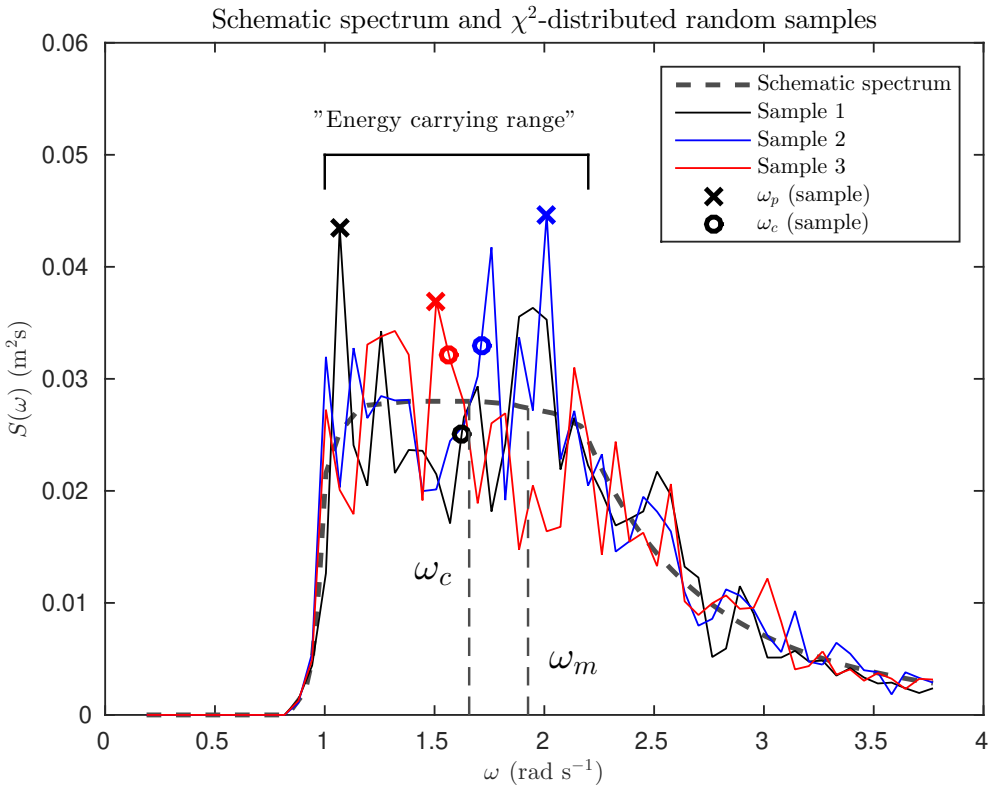

Figure 4.1: A schematic archipelago-type spectrum. The three sample spectra are numerically generated from the schematic spectrum using a χ^2-distribution with 31 degrees of freedom. ω_m is the mean frequency and ω_c is the characteristic frequency (Eq. 2.21).

The dominant wind sectors in the GoF are from south-east/east and from south-west. Fig. 4.2 illustrates wave spectra that were generated by winds from these dominant sectors in four different areas: the Open sea, the Outer archipelago, the Transition zone, and the Inner archipelago. These areas were represented by one measurement site each (GoF, O1, T2, and I3 respectively). Each case contained 7–11 spectra and had a mean wind speed of 11–13 m s^{-1}. The spectra for the Open sea and the Transition zone were coinciding, as were the spectra for the Outer and Inner archipelago.

In Paper III the spectral shape in the Transition zone was found to depend strongly on the wind direction because of the anisotropic fetch and bottom conditions. This variation was also evident when comparing the spectra generated by south-westerly winds (left column) and south-easterly winds (right column) (Fig. 4.2). In the Open sea the easterly winds produced a more peaked spectrum, since the westerly fetch geometry resulted in a stronger disagreement between the fetch restricting the growth of the peak frequency and the fetch restricting the growth of the total wave energy, as found by Kahma and Pettersson (1994). A similar difference was seen in the Outer archipelago, where the waves generated by the south-westerly winds were affected by the Porkkala peninsula, as noted in Paper I. The general trend, however, was the widening of the spectrum when moving into the archipelago towards the shore.

In the Transition zone the strong sheltering by islands in the east (especially Isosaari) resulted in a wide spectrum, while the nearshore Inner archipelago site was sheltered in such a way for both dominant wind directions. The spectral shape in the Transition zone during easterly winds was close the ideal archipelago spectrum in Fig. 4.1, as was the spectra in the Inner archipelago. The low κ^2 narrowness values (0.01–0.03) agreed with this visual assessment. Nonetheless, the energy carrying range in the Transition zone's extended to lower frequencies than in the Inner archipelago because of the higher exposure to open-sea waves.

4.2 The spectral tail

The equilibrium values of the spectra in Fig. 4.2 agreed with $\alpha_u = 3.3 - 4.5 \cdot 10^{-3}$ found by Kahma (1981) and Kahma (1986) (Fig. 4.3). The open sea GoF buoy had larger equilibrium levels compared to the more sheltered locations, with the exception of the easterly wind case in the Transition zone. Since the wave buoys could not measure waves shorter than 3.6 rad s^{-1} (0.6 Hz), they were complemented with high-frequency wave staff measurements from R/V *Aranda* (Paper IV). The wave staff spectra from the open sea (sites 15031 & 15035) had equilibrium values of $\alpha_u \approx 4.5 \cdot 10^{-3}$. These spectra transitioned from ω^{-4} to ω^{-5} around $\omega U/g = 4 - 5$, which is in the frequency range where the wave buoys measurements ended. The wave staff spectra had only a short ω^{-5} range before transitioning back to an ω^{-4} power-law. This second ω^{-4} range had lower equilibrium values and was observed to continue to at least $\omega U/g = 20$ (Paper IV).

The only high-frequency measurements from the archipelago (site 15033 in the Archipelago Sea, Fig. 1.4) were compared to wave buoy data gathered roughly 160 km away in the Helsinki archipelago (site I3, Fig. 1.3). The shortest fetch at 15033 was about 2 km, with a 15 km narrow passage to the south. The shortest fetch at I3 was around 1.5 km, but

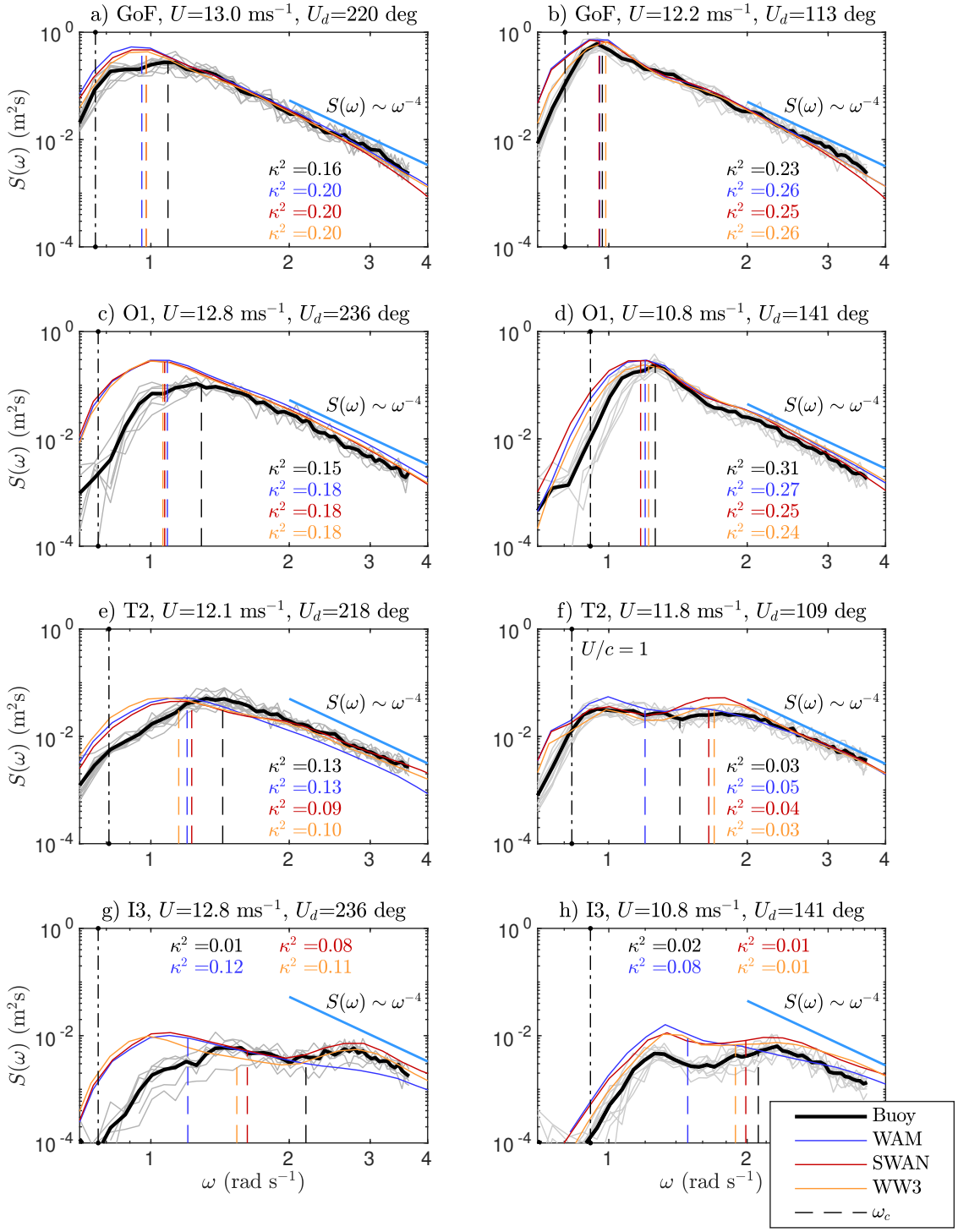

Figure 4.2: Observed and modelled wave spectra at four locations off Helsinki (see Fig. 1.3) for south-westerly (left column) and easterly (right column) winds. The vertical dashed lines shows the characteristic frequency integrated up to 0.58 Hz (see Eq. 2.21).

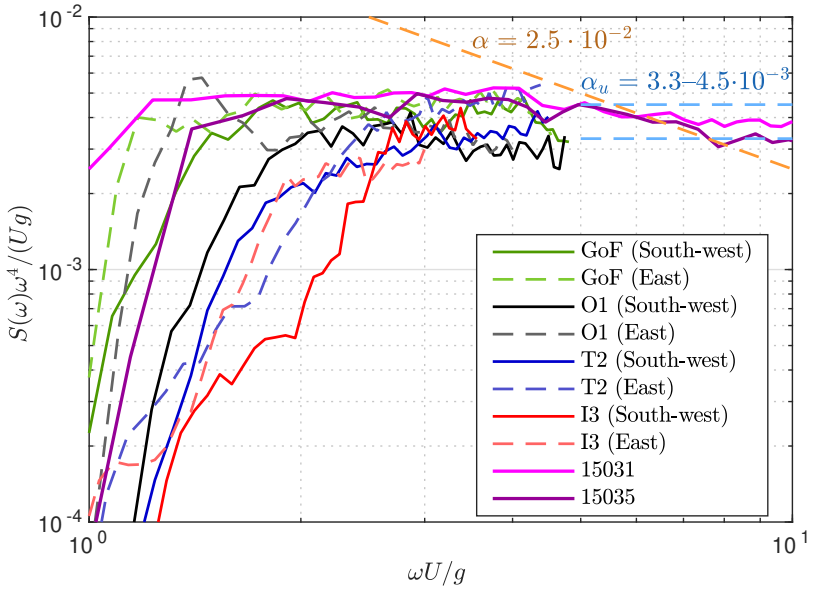

Figure 4.3: The wave buoy spectra from Fig. 4.2 plotted with an equilibrium normalisation along high-frequency spectra obtained at the mouth of the GoF (15031) and the Bothnian Sea (15035) with R/V *Aranda*.

it was exposed to attenuated open sea waves propagating from the Gulf of Finland.

Wave spectra for 2 hours were compared (Fig. 4.4 a). The mean wind speed measured at R/V *Aranda* was between 9.6 and 7.6 m s^{-1} (mean 8.6 m s^{-1}). There exists no wind measurements at location I3, but the wind speed at Harmaja was 9.0–9.9 m s^{-1} (mean 9.5 m s^{-1}). The wind speed at Kruunuvuorenselkä was approximately 8.7 m s^{-1} (a proportionality constant 0.91 determined through linear regression). Kruunuvuorenselkä is slightly more exposed than I3, and 8.7 m s^{-1} was used as an upper estimate. The wind speed at an inland weather station (Kaisaniemi) was only 3.2 m s^{-1} during the I3 measurements. The wind speed interpolated linearly between Harmaja and Kaisaniemi was 5.6 m s^{-1}, which will serve as a lower bound. The best estimate for the wind speed at I3 was therefore 7.1 m s^{-1} ($\pm$ 1.5 m s^{-1})—about 75% of the wind speed at Harmaja.

The wave spectra from the two locations agreed well up to the Nyquist frequency of the wave buoy after being scaled with the wind speed. The energy below $\omega = 2.4$ rad s^{-1} was missing in the wave staff measurements because site 15033 wasn't exposed to open sea waves. In the wave staff measurements only a short ω^{-5} range was visible before a transition to a second ω^{-4} range (Fig. 4.4). The high-frequency spectra were mostly described by an ω^{-4} tail (shown up to 10 rad s^{-1}), which is similar to the open sea spectra in Fig. 4.3.

The data in Paper IV, Fig. 4.3, and Fig. 4.4 suggest that the rear face of the spectrum has a similar structure both in the archipelago and the open sea. Still, more high-frequency measurements from archipelago conditions are required to confirm this conclusion.

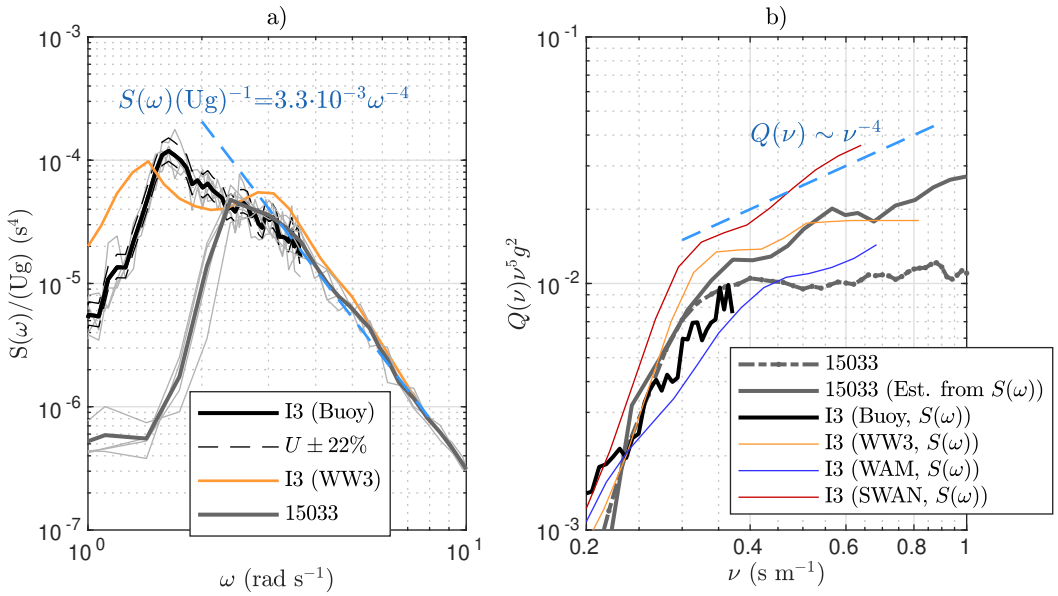

Figure 4.4: Wave spectrum from I3 in the Helsinki archipelago (18 Oct 2012, $U = 7.1 \pm 1.5$ m s^{-1}), and a high-frequency spectrum from 15033 in the Archipelago Sea roughly 160 km away (09 July 2015, $U = 8.6$ m s^{-1}). Panel a) shows the wave spectra normalized by Ug. Panel b) shows the inverse phase-speed saturation spectra (not scaled with U). Solid lines in panel b) are estimates calculated from the frequency spectra.

4.2.1 Wavenumber and inverse-phase speed spectra

The equilibrium-to-saturation transition in the Archipelago Sea wavenumber spectra took place at roughly $kU^2/g = 10$, which is $U/c = \sqrt{10} = 3.2$ if deep water linear theory is assumed. This transition point agreed with $U\nu = U/c = 3$, which was identified in the inverse phase-speed spectra (Fig. 11 in Paper IV). Still, the equilibrium range in the frequency domain typically didn't end before $\omega U/g = U/c = 4 - 5$, even extending up to $\omega U/g = 8 - 9$ for strongly forced spectra.

Unlike the short ω^{-5} range in the frequency domain, both the wavenumber and the inverse phase-speed spectra had a clear k^{-3} (and ν^{-5}) saturation range. The saturation constants determined from the wavenumber and inverse phase-speed domains also agreed well, being $\alpha/2 = F(k)k^3 \approx 6 \cdot 10^{-3}$ and $\alpha = Q(\nu)\nu^5 g^2 \approx 1 \cdot 10^{-2}$ (the latter shown in Fig. 4.4b). The saturation constant determined from the frequency spectra was roughly twice as large, which was consistent with Forristall (1981).

The incompatibility between the wavenumber and frequency domains has been previously identified by Wang and Hwang (2004) and Lenain and Melville (2017). In Paper IV the main reason for the discrepancies was determined to be wave non-linearities. The Doppler shift, as proposed by e.g. Banner (1990), was excluded as a leading explanation, since it would also have affected the inverse phase-speed spectra, thus breaking the agreement between the k^{-3} and ν^{-5} saturation regimes.

4.3 The characteristic wave frequency, ω_c

The peak frequency is practically undefined in an archipelago-type spectrum with a broad energy carrying range (Fig. 4.1). The strong scatter makes the peak frequency less useful in assessing wave model performance (Paper II), but it is also questionable to which degree it actually characterizes the wave field in archipelago conditions (Paper III).

In Paper III a more stable characteristic frequency, ω_c, was defined using the integral in Eq. 2.20 with $q = 4$; this expression has been proposed as a definition for the peak frequency by Young (1995). For more exposed location the characteristic frequency was close to the spectral peak (Fig. 4.2), while being slightly biased for wave growth affected by a narrow fetch geometry (Paper III). The advantage over the mean frequency was that ω_c quantified the centre of the energy carrying range in an archipelago type spectrum (Fig. 4.1, Fig. 4.2f). The characteristic frequency can thus be though of as a generalization of the peak frequency, since it is equivalent to the peak frequency for narrow spectra.

4.4 Implications for wave height parameters

4.4.1 Highest individual waves and $H_{1/3}$

The traditional definition of the significant wave height is the mean of the highest one-third of the individual waves ($H_{1/3}$, Eq. 2.16). By assuming deep water, Gaussian water level displacements, and a narrowbanded spectrum, it follows that the individual wave heights would be Rayleigh distributed with a parameter of $\sqrt{4m_0}$, where m_0 is the variance of the wave field (Longuet-Higgins, 1952). Since the variance is more easily calculated than the height of every single wave, these two definitions for the significant wave height were connected on a theoretical basis as:

$$H_{1/3} = 4\sqrt{m_0} \Leftrightarrow H_{1/3}/H_{m_0} = 1. \tag{4.1}$$

Experimental studies have found that the above equality doesn't hold precisely. Forristall (1978) determined the ratio $H_{1/3}/H_{m_0}$ to be 0.942 using storm wave data. Longuet-Higgins (1980) used a scaled Rayleigh distribution of $\alpha_R\sqrt{4m_0}$ and found $H_{1/3}/H_{m_0} = \alpha_R = 0.925$ for the data of Forristall (1978). Longuet-Higgins (1980) found the coefficient α_R to depend on the spectral width; it is therefore expected that the ratio $H_{1/3}/H_{m_0}$ would be smaller than $\approx 0.93 - 0.94$ in the archipelago where the wave spectra are wide.

The open sea GoF data was in good agreement with previous studies, with $H_{1/3}/H_{m_0} = 0.927$. The ratio determined from the data in the Transition zone (T2) was only $H_{1/3}/H_{m_0} = 0.881$, which indicated a decrease in the highest wave height compared to the standard deviation $\sqrt{m_0}$. The single highest wave at T2 was, on average, $H_{max}/H_{m_0} = 1.58$, which was lower than 1.68 predicted by Forristall (1978). It was also lower than the respective value determined from the GoF open sea data (1.61).

The predictions based on the Rayleigh-type distributions determined in previous studies overestimated the height of the highest single wave in the archipelago (Table 3 in Paper III). Paper III found that the finite water depth didn't explain the differences between the results in the archipelago and the open sea. The results were best explained by the wider

spectral shape, and linear fits to the narrowness parameter κ^2 resulted in the equations:

$$H_{1/3}/H_{m_0} = 0.85 + 0.15\kappa^2 \quad (4.2)$$
$$H_{max}/H_{m_0} = 1.57 + 0.27\kappa^2. \quad (4.3)$$

The deviations from the theoretical results of Longuet-Higgins (1952) were therefore determined to be caused by the violation of the narrowbanded assumption, not the deep water assumption. Indeed, for a narrowbanded spectrum ($\kappa^2 \to 1$) both equations agreed with the theoretical results of Longuet-Higgins (1952) (Table 3 in Paper III). A lot of scatter still exists, with the correlation coefficients being only $r = 0.64$ (Eq. 4.2) and $r = 0.15$ (Eq. 4.3).

4.4.2 Confidence intervals

According to Donelan and Pierson (1983), the degrees of freedom of the total wave field variance, m_0, depend on the spectral shape in the following way:

$$\text{d.o.f.}(\hat{m}_0) = \frac{l\left[\sum_{i=1}^{N}\hat{S}(\omega)\right]^2}{\sum_{i=1}^{N}\left[\hat{S}(\omega)\right]^2}, \quad (4.4)$$

where l is the degrees of freedom of one frequency bin in the wave spectrum, and $\hat{S}(\omega)$ underlines that the spectrum is a sample. Since a single spectral bin is χ^2_l-distributed, also $\hat{m}_0$ will be χ^2-distributed with the degrees of freedom of Eq. 4.4. Thus, for k=d.o.f.($\hat{m}_0$):

$$\hat{H}_{m_0} = H_{m_0}\sqrt{\frac{\chi^2_k}{k}}. \quad (4.5)$$

The confidence limits for the measured significant wave height in the open sea (GoF) were, on average, up to 50% higher than for the wider spectra of the archipelago (Table 2 in Paper III). Following Table 2 in Paper III, the confidence limits in the Transition zone (T2) can be calculated by using $k = 410$. Still, the degrees of freedom varied with the wind direction, being only 250 for the more peaked spectra generated by southerly winds (Fig. 4 a in Paper III).

5 The modelled archipelago wave field

5.1 The wave spectrum

The three wave models mostly reproduced the wave spectra well, which was also reflected in the general agreement between the measured and modelled κ^2 values (Fig. 4.2). The largest discrepancy was the overestimated energy for south-westerly winds in the Outer archipelago (Fig. 3 in Paper I & Fig. 4.2c). This behaviour was identified for WAM at location O1 in the Outer archipelago (Paper I), and the bias persisted at location O3, located 13 km south-west of O1 (Paper II). Paper II also found that SWAN and WW3 behaved like WAM in the Outer archipelago despite having different numerical schemes and parameterizations of the physical processes. The long-wave energy that was overestimated in the models for south-westerly winds propagated through the Transition zone to the Inner archipelago (Fig. 4.2g).

All models captured the wave spectrum more accurately during easterly winds (Fig. 4.2, right column). WAM showed a slight tendency to overestimate the low-frequency energy inside the archipelago, while SWAN and WW3 overestimated the local wave growth (Fig. 4b in Paper II). The same tendencies were found in the Inner archipelago point I3 (Fig. 4.2h). Nonetheless, the discrepancies with the measurements were smaller than for south-westerly winds.

The rear face of the spectrum was also mostly simulated well by the models. The main exception was found in the Transition zone, where WAM and WW3 modelled too little energy in the spectral tail during south-westerly winds even though SWAN reproduced the high-frequency part of the spectrum correctly (Fig. 6a in Paper II & Fig. 4.2e). In the Inner archipelago WAM underestimated the local wind sea, which was captured well by SWAN and WW3 (Fig. 4.2g).

The simulated wave spectra in the inner Helsinki archipelago were also compared with high-frequency wave staff measurements from the Archipelago Sea, as presented in Sect. 4.2 (Fig. 4.4). The observed tail mostly followed an ω^{-4} power law (as assumed in SWAN). The shape of the tail in WW3 were in good accord with the wave staff measurements, although the energy levels were slightly too high. WW3 adds a diagnostic ω^{-5} tail for the highest frequencies, which was consistent with the short transition seen in the wave staff measurements. The inverse phase-speed spectrum showed a ν^{-5} saturation, which is theoretically consistent with a continued ω^{-5} tail if non-linearities are assumed weak.

5.2 Bulk wave parameters

All three models agreed on the significant wave height, which was simulated well inside the archipelago (Paper II). The modelled wave height was slightly too large at the locations closest to the shore, but the most significant bias was in the Outer archipelago at O1 and O3, as discussed in Sect. 5.1. The small intermodel variations in spectral shape did not translate into notable differences in the significant wave height.

The validation of the peak period, T_p, was very challenging because of its instabil-

ity in archipelago conditions (Paper II). The slight differences in how the three models simulated the wave spectrum were visible in the peak period in a mean sense: SWAN and WW3 had a negative bias, since they more consistently determined the peak period to be that of the shorter, locally generated, waves; WAM had a positive bias in the peak period because of the overestimation of the longer waves. Still, if only the peak period is validated, the disparities appear greater than the actual small differences between the model spectra (Fig. 4 in Paper II, and Fig 4.2 f).

The characteristic frequency, ω_c, agreed with the measurements for easterly winds at the GoF and O1 (Fig. 4.2). For south-westerly winds the bias roughly corresponded to the difference in peak frequencies. Inside the archipelago the discrepancy between the measured and modelled characteristic frequency reflected the low- or high-frequency bias' of the model. The combined information from the significant wave height (H_s), the characteristic frequency (ω_c), and the spectral narrowness parameter (κ^2) gave a good grasp on how well the wave spectrum was modelled.

5.3 The wind forcing and the bathymetry

Paper I validated the NWP systems HIRLAM and HARMONIE against the open sea Kalbådagrund station and the Harmaja station (Fig. 1.3). The same models were validated in Paper II also against measurements from Helsingin majakka and Kruunuvuorenselkä. The newly acquired measurements from the Kruunuvuorenselkä research station provided the first opportunity to validate NWP-systems in this area of the Helsinki archipelago.

The operational HIRLAM products were sufficient to force the wave models in the archipe-lago, even though the spatial resolution was an order of magnitude coarser compared to the wave models (7.4 km vs 0.185 km). The higher resolution HARMONIE model outperformed HIRLAM only at Kruunuvuorenselkä in the archipelago. Nevertheless, the results of the coarser HIRLAM were adequate even in this area (Table 4 in Paper II).

Increasing the temporal resolution of the wind forcing from 3 h to 1 h improved the quality of the wave simulation. The impact was determined from the variance density spectrum calculated from the significant wave height time series at T2 (Fig. 5.1). This spectrum of H_s is denoted $\mathcal{H}_s(f)$ (m^{2}h) to distinguish it from the wave spectrum. The frequency, f, had units h^{-1}, and the spectrum above (24 h)$^{-1}$ followed an f^{-3} power law. The WAM-simulation that used the 1 h HARMONIE winds matched the observations up to (3 h)$^{-1}$, but the fastest variations in significant wave height weren't captured when WAM was forced with 3 h HIRLAM winds (Fig. 5.1a).

The tail of $\mathcal{H}_s(f)$ was dominated by the statistical variability of the observed significant wave height. Thus, the discrepancy with WAM-HARMONIE above (3 h)$^{-1}$ was not a shortcoming of the model. Adding a simulated χ^2-variability to the WAM-HARMONIE time series using Eq. 4.5 and 410 d.o.f. (Table 2 in Paper III), the spectrum $\mathcal{H}_s(f)$ calculated from the model time series coincided with the observations (Fig. 5.1b). The WAM-HIRLAM data, again, differed from the observations even with the added simulated variability, meaning that using a 3 h time step in the wind forcing loses some variations in the wave field that would be possible to capture with a numerical wave model.

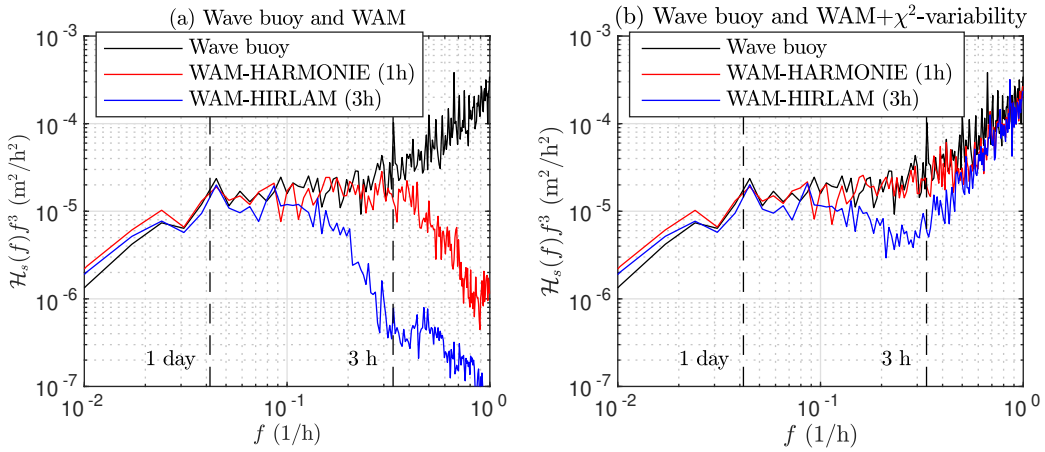

Figure 5.1: The variance density spectra, $\mathcal{H}_s(f)$, of the H_s data in the Transition zone. Panel (a) shows the spectrum (multiplied by f^3) of the wave buoy data, and spectra of the WAM data that were produced with an hourly wind forcing (HARMONIE) and with winds available every third hour (HIRLAM). Panel (b) shows the same data, but with a simulated χ^2-variability added to the model data. The spectra have been calculated from the 2016 significant wave height data at location T2.

Accurate bathymetrical information is important for the model performance, and this aspect was explored in Paper I. The two high-resolution bathymetrical grids used in the WAM simulations produced almost identical results. Also the influence of the bottom related processes were small in the Outer archipelago, suggesting that small variations in the bathymetrical information were not responsible for the observed errors in the Outer archipelago. The accuracy of the available bathymetrical information was deemed sufficient for the purposes of wave modelling in archipelagos.

6 Discussion

6.1 Parameterizing the archipelago spectrum

Traditionally the omnidirectional wave spectrum has been described by its peak frequency and total energy. The energy has been quantified either directly, or e.g. through the value of the constant α in the JONSWAP spectrum. While the fetch geometry has been found to influence the relationship between the energy and the spectral peak, the spectra affected by narrow and slanting fetch have still been well described as less peaked versions of traditional spectra (Pettersson, 2004).

In archipelago conditions two issues exist: i) there is a need to quantify the width of the spectrum, ii) the peak frequency is ill-defined. The archipelago spectra with their wide energy carrying regions can no longer be fitted to traditional spectral parameterisations by modifying the peakedness parameter (Fig. 4.1). The width of this energy carrying range is also not constant, as readily seen when comparing panels f) and h) in Fig. 4.2. It therefore follows that the the low-frequency part of the archipelago spectrum cannot be parameterized as a fixed modification to any existing spectral model. The spectral width was successfully quantified using the κ^2 narrowness parameter (Battjes and van Vledder, 1984); the width parameter ν_{LH} by Longuet-Higgins (1980) had no descriptive value in the data set of this study.

In this study the characteristic frequency, ω_c, was proposed to describe the archipelago spectrum instead of the ill-defined peak frequency. In the archipelago ω_c was roughy representative of the middle of the energy carrying range, which is a defining property of the archipelago type spectrum. It also reverted to an unbiased estimate of the peak frequency for narrow spectra, which is why this definition was originally proposed as an alternative definition for the peak frequency by Young (1995).

The triplet $(m_0, \omega_c, \kappa^2)$ can serve as a starting point for a parameterization of the archipela-go spectrum. Wave spectra inside the archipelago typically show no overshooting, but the γ peakedness parameter would need to be retained if the parameterization should cover also traditional fetch-limited spectra. Nevertheless, it is entirely possible that some other width parameter will turn out to be more useful. A way to reliably define the upper frequency of the energy carrying range might also be needed, since it represents the peak frequency of the shortest fetch, and thus the start of an ω^{-4} rear face. It might even turn out that an additional parameter must be added to account for the possible slope within the energy carrying range. The construction of a parameterization that would cover the entire transition of the spectrum (Fig. 2 in Paper III) is a formidable challenge that wasn't solved in this study.

6.2 Individual wave heights

If we assumed a universal distribution, the number of waves in a time series would determine the expected maximum height of a single wave. The shorter wave periods in the archipelago (compared to the open sea) would mean a larger number of waves, and thus a higher expected maximum wave. Yet, the exact opposite was found. The decrease in the

height of the single waves, with respect to the significant wave height H_{m_0}, for a wider spectrum has been proposed to be caused by the de-correlation of following crests and troughs (Casas-Prat and Holthuijsen, 2010). This explanation was supported by the data in this study, since the maximum wave crests η_{max}/H_{m_0} determined from the open sea data (0.93) and the archipelago data (0.92) were consistent. The crest heights also followed Casas-Prat and Holthuijsen (2010) and the theoretical results of Longuet-Higgins (1952).

The ratio $H_{1/3}/H_{m_0}$ depended on the spectral narrowness κ^2, but with a significant amount of scatter. The dependence on the spectral width were in line with Longuet-Higgins (1980), who scaled the assumed Rayleigh distribution—and thus $H_{1/3}/H_{m_0}$—using the spectral width coefficient, ν_{LH}. Also Vandever et al. (2008) found a similar connection between ν_{LH} and $H_{1/3}/H_{m_0}$.

Vandever et al. (2008) found no dependence of the highest single wave with respect to the significant wave height and the spectral width ν_{LH}, possibly because the authors used $H_{1/3}$ instead of H_{m_0}, thus scaling the single highest waves with the mean of the highest waves. In Paper IV a connection between H_{max}/H_{m_0} and κ^2 was established with a weak correlation ($r = 0.15$). Despite the scatter, Eq. 4.2 and Eq. 4.3 are consistent with the theoretical results of Longuet-Higgins (1952) for a very narrow spectrum ($\kappa^2 \approx 1$). It is still unclear if the poor correlation was caused mainly by the difficulty to define a good metric for the spectral width, and it is therefore possible that the scatter could be reduced by choosing a different width parameter.

The different behaviour of the crest heights and the wave heights are important for practical applications. The maximum crest height is relevant for e.g. wave overtopping, while the safety of vessels are threatened by large wave heights. In archipelago conditions the ratio between the wave height and the crest height varied with the spectral width, which needs to be accounted for if results from observations are generalized to cover larger areas.

6.3 The rear face in different spectral domains

The existence of both a wind-dependent ω^{-4} (or $k^{-2.5}$) equilibrium range and a constant ω^{-5} (or k^{-3}) saturation range has theoretical and experimental support (Phillips, 1958; Kitaigorodskii, 1962; Hasselmann, 1974; Kahma, 1981; Forristall, 1981; Kitaigorodskii, 1983; Romero et al., 2010; Tamura et al., 2014). Nevertheless, the behaviour of the two spectral domains have not been consistent when comparing the frequency and the wavenumber spectrum from spatio-temporal measurements (Wang and Hwang, 2004; Lenain and Melville, 2017). Lenain and Melville (2017) found that the wavenumber spectra transitioned to a saturation regime, while the frequency spectra did not. Results to this affect were also obtained in Paper IV.

Kitaigorodskii et al. (1975) and Banner (1990) attributed the distortion of the hypothetical ω^{-5} power-law to currents and Doppler effects by the orbital velocities of longer waves. Later studies have highlighted the role of higher order harmonics, and determined the Doppler distortion caused by the orbital motion of longer waves to be comparatively small (Wang and Hwang, 2004; Janssen, 2009; Leckler et al., 2015; Guimarães, 2018).

In Paper IV the good agreement between the inverse phase-speed spectra (subject to the Doppler shift) and the wavenumber spectra (not subject to the Doppler shift) offered more experimental support for the importance of wave non-linearitites.

For the fetch-limited data from the Archipelago Sea the equilibrium levels varied less in the inverse phase-speed spectrum compared to the frequency spectrum. This disagreement raises the question if the U/c_p dependence of α_u (found by Donelan et al. (1985)) is a real intrinsic part of the wave field, or if it is mainly an artefact of the stronger higher order harmonics that are caused by the steeper waves.

Leckler et al. (2015) attacked the problem with non-linearitites by removing the higher order components from the frequency spectrum, thus determining the first order spectrum. A fundamental question is: are wave models simulating the frequency spectrum or the first order spectrum? Both source terms and the wave propagation are calculated assuming linear wave theory, or in essence that the frequency spectrum is the same as the first order spectrum. These models are then tuned and validated mostly against frequency measurements, which have been distorted by wave non-linearities.

In the case of parameterizing the energy input from the wind, the determining factor is U/c, which in a (deep water) model is $U\omega/g$. This implicitly assumes that all the energy in the frequency ω travels with the speed of the free harmonic, which is not the case (Hara and Karachintsev, 2003; Wang and Hwang, 2004; Leckler et al., 2015). The wind input at $U\omega/g$ will be different for the first order spectrum and the full frequency spectrum. Since the harmonics make up one physical wave, their common attribute is therefore their phase speed. The discrepancy is solved if the inverse-phase speed spectrum is used, since the spectrum $Q(\nu)$ contains the energy all harmonics that have a phase speed ν^{-1}. Nonetheless, the Q-spectrum have to be based on measurements of the phase speed; estimating it from the frequency spectrum, $S(\omega)$, adds no new information.

The presence of ambient currents will affect the inverse phase-speed measurements. This is not a problem when quantifying the wind input, since the relevant reference frame is relative to the wind. When quantifying dissipation caused by wave breaking, the relevant reference frame is intrinsic, which favours the use of the wavenumber spectrum. If the full wave spectrum is available, all three spectra—$S(\omega)$, $F(k)$, and $Q(\nu)$—can be directly calculated; they are all distinct representations of the wave field in the sense that none of them can be converted to the other (without theoretical simplifications). They all have value in describing different aspects of the wave field, and the question becomes choosing the right tool for the particular application at hand.

6.4 Modelling challenges

All results of the models were representative only of their chosen set-ups. Preliminary comparisons—where the source terms were used ”out of the box” without any additional tuning—showed that the ST4 package (Ardhuin et al., 2010) agreed best with the data in this study. Nonetheless, SWAN, and especially WW3, has many different source terms (e.g. Tolman and Chalikov, 1996; van der Westhuysen et al., 2007; Zieger et al., 2015), and choosing different ones could significantly alter the results. Changing the propagation scheme could also affect the simulations, but probably to a lesser extent (Perrie et al.,

2017).

The common issue found in all three models was the overestimated significant wave height for south-westerly winds in the Outer archipelago points that were partially sheltered by the Porkkala peninsula (Paper I and II). The behaviour persisted when using different wind forcings, bathymetrical data, propagation schemes, and source terms. The wave field was made up by two wave systems with slightly different directions, both travelling slower than the wind. Still, the measured spectrum was not unimodal, while the modelled spectrum was (Fig. 4 in Paper I). One possibility is that DIA could not capture the interaction between these to actively forced wave systems accurately enough, which should to be tested with simulations calculating the interactions exactly (e.g. van Vledder, 2006).

In the archipelago WAM underestimated the energy of the spectral tail for south-westerly winds, and a similar (but weaker) tendency was observed for WW3 (Fig. 4.2 e & g). SWAN was implemented with the oldest physical parameterization of the wind input (Komen et al., 1984; Wu, 1982), but still outperformed the other models in this specific aspect. Both WAM and WW3 were implemented with a wind input where the wave-supported stress was determined from the wave spectrum. As noted by Ardhuin et al. (2010), this type of parameterizations are highly sensitive to the highest frequencies. Higher energy levels in the tail will increase u_*, which will in turn further increase the energy in the spectral tail through the positive feedback.

Paper II found that the friction velocity in WAM and WW3 were lower when the high-frequency energy was underestimated (using u_* by SWAN as a benchmark). The older wind input of SWAN was immune to this aforementioned feedback mechanism, thus providing a certain robustness inside the archipelago. It is possible that the determination of the wave-supported stress was influenced by the excess long wave energy, thus decreasing the friction velocity. The sheltering term in the parameterization of Ardhuin et al. (2010) might have partially compensated for the unwanted feedback, which would explain why WW3 performed slightly better than WAM. Nevertheless, no friction velocity measurements were available in the Helsinki archipelago, which means that there was no way of saying to what degree the friction velocity was under/overestimated by any of the models.

The ST6 source term package in WW3 (Zieger et al., 2015) was recently re-tuned by Liu et al. (2019), and it was found to reproduce an ω^{-4} to ω^{-5} transition well. Validating this updated source term package against the measurements of Paper II—and the continued measurements at T2—would be a useful study into the modelling of the rear face of the spectrum in the archipelago. Ideally, the continued measurements at T2 in the Transition zone would be accompanied with a field campaign collecting friction velocity measurements and high-frequency wave data.

The resolution of the atmospheric forcing has been found to be important for the accuracy of the wave simulations (Cavaleri and Bertotti, 2004; Tisler et al., 2007), but our results indicated that a 7.5 km wind product was adequate to force the wave simulations in the archipelago. Nonetheless, the lack of a proper land mask (Fig. 1 in Paper I) is one aspect that might still restrict the potential of the high-resolution HARMONIE model in the archipelago.

A coarse temporal resolution of the forcing wind data (3 h) restricted how well the

wave model captured fast variations in the wave field, while a 1 h temporal resolution mostly missed only the statistical measurement variability (Fig. 5.1). WAM-HARMONIE (1 h) captured 87 % of all variations of a time scale between 2 h and 10 h. The same number for WAM-HIRLAM (3 h) was only 45 %.

Paper I was based on regular grids since unstructured grids are not available in WAM. Although unstructured grids are possible both in SWAN and WW3, all models were implemented with structured grids for Paper II to allow for a comparison with the results in Paper I. Generally, the 0.1 nmi structured grid implementations performed well. Tuomi et al. (2014) found that the low-frequency energy modelled with a 0.5 nmi structured grid was improved when creating sub-grid obstructions using 0.1 nmi data; the land-sea mask with an 0.1 nmi accuracy was accounted for explicitly in the grid of this study. Nonetheless, it is possible that the results could possibly be improved by using even higher spatial resolutions either directly or as sub-grid obstructions. Building an unstructured grid would also be an attractive goal, but the very complex coastline and small islands makes the generation of unstructured meshed in archipelagos difficult. A compromise might be achieved by using structured grids with adaptive resolutions. Such a feature has been have been added to WW3 (SMC, Li, 2011), and it works like an automatic ”on-demand” nesting of areas where a higher spatial resolution is required.

7 Conclusions

The wave field in the archipelago was studied. The observations consisted of extensive wave buoy measurement from the Helsinki archipelago in the Gulf of Finland, Baltic Sea, and high-frequency wave staff measurements from R/V *Aranda*, part of which were from the Archipelago Sea. Wind data were provided by four automatic weather stations in the GoF and a Sonic anemometer on R/V *Aranda*. The wave field in the Helsinki archipelago was also modelled using three state-of-the-art, high-resolution, numerical wave models. The models were forced by winds from two numerical weather prediction (NWP) systems with different resolutions. The material was used to study the properties of the wave spectrum, namely how it evolves through the archipelago and how well different parts of the spectrum can be reproduced by the numerical models.

The measurements from R/V *Aranda* were used to study the equilibrium and saturation ranges and their transition point in the rear face of the spectrum. The Wavelet Direction Method (WDM) was used to extract wavenumber spectra from the wave staff data. A new, previously undefined, inverse phase-speed spectrum was also defined, formulated, and studied. This spectrum is denoted $Q(\nu)$, where $\nu = |\boldsymbol{\nu}|$ is the modulus of the inverse phase-velocity $\boldsymbol{\nu} = \boldsymbol{k}\omega^{-1}$.

The main conclusions of this study are the following:

1. The wave spectra in the archipelago differed significantly from the unimodal shape observed in the open sea. A unimodal shape was still visible in the outer edge of the archipelago, but inside the archipelago, close to the shore, the spectral shape was flat. The flat shape of the archipelago spectrum was characterized by a broad frequency range where the spectral density was almost constant ("the energy carrying range"). The results of the study were grouped to make them more presentable, but the transition was in reality more continuous; the spectral shape in the middle of the archipelago varied between the above mentioned extremes, depending only on the amount of sheltering present for different wind directions. The tail of the archipelago spectrum mostly followed an ω^{-4} power law in the frequency domain in both the wave buoy observations and the high-frequency wave staff observations—for this part the archipelago spectra agreed with the open sea measurements.

2. The flat shape of the wave spectrum in the archipelago made the peak frequency ill-defined, since the statistical variability in the energy carrying range introduced strong scatter. An integrated mean frequency weighted by $S(\omega)^4$ was proposed as a new "characteristic" frequency, ω_c, to be used over varying wave conditions throughout the archipelago. For an archipelago type spectrum ω_c quantified the centre of the energy carrying range, while it was an unbiased estimate for the peak frequency for waves growing from a straight shoreline. Young (1995) proposed the expression with $q = 4$ as an alternative definition for the peak frequency, but substituting $\omega_p := \omega_c$ cannot be recommended for waves growing in a narrow fetch geometry or in the archipelago. Rather, ω_c can be used as an additional frequency parameters with desirable limiting properties for both narrow and wide spectra.

3. The spectral significant wave height (H_{m_0}) and the traditional mean-of-the-highest-third ($H_{1/3}$) disagreed strongly in the middle of the archipelago. The average value was determined to be $H_{1/3} = 0.881 H_{m_0}$ using a linear fit, while the respective value for the highest individual wave was $H_{max} = 1.58 H_{m_0}$. Both these ratios were lower than results determined using open sea data. The reason for the differences to open sea measurements was determined to be the increase in spectral width, not the finite water effects; the results varied as a function of the spectral peakedness κ^2, although especially the H_{max}/H_{m_0} data had strong scatter.

4. The numerical wave models—WAM, SWAN, and WAVEWATCH III® —all simulated the significant wave height well in the archipelago with the configurations chosen in this study. In the archipelago the dominant peak in the measured wave spectrum varied randomly within the energy carrying range. The numerical models determined the peak period in a more deterministic fashion by favouring some part of the energy carrying range; SWAN typically simulated more energy in the higher frequency part of the energy carrying range, while WAM was biased toward the lowest frequencies. Despite the quite accurately simulated wave spectra, the statistical variations in the energy carrying range caused poor scatter statistics and a strong (positive or negative) bias for the modelled peak period. The largest inaccuracy in the simulated wave field was found in the Outer archipelago, where all models overestimated the wave energy significantly for locations partially sheltered by a peninsula. Inside the archipelago the wave models also underestimated the high-frequency wave energy, in certain conditions, when implemented with wind-input source terms that determined the wave supported stress from the wave spectrum.

5. The operational wind products were adequate for forcing the high-resolution coastal wave models even though the discrepancy between the spatial resolutions were one order of magnitude. The higher resolution atmospheric forcing performed better than the coarser operational product only when compared against newly acquired wind measurements close to the coast inside the archipelago. A coarse temporal resolution (3 h) of the wind forcing limited how well the variations in the time scale of 2–10 hours were modelled, while shorter variations disagreed with the measurements also when using hourly forcing data. Nevertheless, the fastest variations were dominated by the statistical variability of the measurements, which a numerical wave model does not even attempt to reproduce. Thus, it can be concluded that all variations in the significant wave height—that are within the realm of the model to simulate—can be captured by using hourly wind forcing data. Even though the existing operational products are adequate, the further development of high-resolution atmospheric models can reasonably be expected to increase the accuracy of coastal wave simulations, especially if the land-sea mask of the archipelago areas are improved.

6. The high-frequency wave-staff data collected in the Archipelago Sea showed that the spectrum saturated to roughly $F(k)k^3 = 6 \cdot 10^{-3}$ at $kU^2/g = 10$. The new inverse phase-speed spectrum was consistent with the wavenumber domain and

showed a saturation to $Q(\nu)\nu^5 g^2 = 1 \cdot 10^{-2}$ at roughly $U\nu = 3$. The transition to a saturation regime was less clear in the frequency spectrum $S(\omega)$, but a transition to $S(\omega)\omega^5 g^{-2} = 2.5 \cdot 10^{-2}$ could be identified at $\omega U/g = 4 - 5$. Nevertheless, at $U\omega/g = 10$ the frequency spectra transitioned back to an ω^{-4} power-law, which continued to at least $U\omega/g = 20$. The equilibrium constant varied less in the Q-spectrum compared to the frequency spectrum, where α_u showed a strong dependence on the strength of the forcing, U/c_p. The main reason for the discrepancies between the wavenumber and frequency domain was concluded to be wave non-linearities, since a strong Doppler effect would have broken the observed consistency between the saturation ranges in the inverse phase-speed and the wavenumber domains.

7. The transition point between the equilibrium and saturation ranges was best described using the inverse wave age, U/c. The speed of the wave component relative to the forcing wind is also a central parameter when calculating the energy input from the wind to the waves. Since the $Q(\nu)$-spectrum gives the apparent (inverse) phase-speed directly from the measurement, no additional current measurements are needed to determine the true relative speed between a wave component and the wind. This might turn out to be a useful feature in future studies. For processes governed by intrinsic wave properties, such as energy dissipation caused by wave breaking, the wavenumber domain should be favoured.

Future work is needed to determine a parameterisation for the wave spectrum that can cover all the different shapes from a peaked to a flat spectrum. This will require additional parameters quantifying the spectral width (e.g. κ^2), and possibly the slope of the energy carrying range.

The first challenge in modelling the wave field in the archipelago was the consistent overestimation of energy in the semi-sheltered areas just outside the archipelago that persisted when using different source terms and propagation schemes; neither could the error be attributed to the bathymetry or the atmospheric forcing. The second challenge was the underestimation of the high-frequency wave energy and the friction velocity in the wind input source term of Janssen (1991)—and to a lesser extent in that of Ardhuin et al. (2010)—under certain conditions in the archipelago. A tuning of these source terms against friction velocity measurements and high-frequency wave data from the archipelago should be performed, but such data are unfortunately sparse.

List of abbreviations

BS	Bothnian Sea
BSBD	Baltic Sea Bathymetric Database
CFL	Courant–Friedrichs–Lewy (condition)
DIA	Discrete Interaction Approximation of the non-linear four-wave interactions
DWR	Directional Waverider
ETOPO	Global relief model of Earth's surface
FFT	Fast Fourier Transform
FMI	Finnish Meteorological Institute
GoF	Gulf of Finland
GPS	Global Positioning System
HARMONIE	A non-hydrostatic convection-permitting atmospheric model
HIRLAM	High-resolution limited area model
IOW	Leibniz Institute for Baltic Sea Research Warnemuunde (Germany)
JONSWAP	Joint North Sea Wave Observation Project
LTA	Lumped Triad Approximation
NWP	Numerical Weather Prediction
R/V	Research Vessel
SHOWEX	Shoaling Waves Experiment
SWAN	Simulating WAves Nearshore
WAM	WAve Model
WDM	Wavelet Directional Method
WW3	WAVEWATCH III®

References

Amante, C. and Eakins, B.W. (2009). *ETOPO1 1 Arc-Minute Global Relief Model: Procedures, Data Sources and Analysis*. Technical report. NOAA. 25 p.

Anderson, J.D., Wu, C.H., and Schwab, D.J. (2015). Wave climatology in the Apostle Islands, Lake Superior. *Journal of Geophysical Research: Oceans*, 120(7), pp. 4869–4890. doi:10.1002/2014JC010278.

Ardhuin, F., O'Reilly, W.C., Herbers, T.H.C., and Jessen, P.F. (2003). Swell Transformation across the Continental Shelf. Part I: Attenuation and Directional Broadening. *Journal of Physical Oceanography*, 33(9), pp. 1921–1939. doi:10.1175/1520-0485(2003)033¡1921:STATCS¿2.0.CO;2.

Ardhuin, F., Rogers, W.E., Babanin, A.V., Filipot, J.-F., Magne, R., Roland, A., van der Westhuysen, A., Queffeulou, P., Lefèvre, J.-M., Aouf, L., Collard, F., and Westhuysen, A.V.d. (2010). Semiempirical Dissipation Source Functions for Ocean Waves. Part I: Definition, Calibration, and Validation. *Journal of Physical Oceanography*, 40(9), pp. 1917–1941. doi:10.1175/2010JPO4324.1.

Babanin, A.V. and Haus, B.K. (2009). On the Existence of Water Turbulence Induced by Nonbreaking Surface Waves. *Journal of Physical Oceanography*, 39(10), pp. 2675–2679. doi:10.1175/2009jpo4202.1.

Banner, M.L. (1990). Equilibrium Spectra of Wind Waves. *Journal of Physical Oceanography*, 20(7), pp. 966–984. doi:10.1175/1520-0485(1990)020¡0966:ESOWW¿2.0.CO;2.

Battjes, J.A. and Janssen, J.P.F.M. (1978). Energy loss and set-up due to breaking of random waves. In: *Proceedings of 16th International Conference on Coastal Engineering*, August 27–September 3, 1978, Hamburg, Germany, pp. 169–587. doi: 10.1061/9780872621909.034.

Battjes, J.A. and van Vledder, G.Ph. (1984). Verification of Kimura's Theory for Wave Group Statistics. In: *Proceedings of 19th International Conference on Coastal Engineering*, Septemver 3–7, 1984, Houston Texas, pp. 642–648. doi: 10.1061/9780872624382.044.

Battjes, J.A., Zitman, T.J., and Holthuijsen, L.H. (1987). A Reanalysis of the Spectra Observed in JONSWAP. *Journal of Physical Oceanography*, 17(8), pp. 1288–1295. doi:10.1175/1520-0485(1987)017¡1288:AROTSO¿2.0.CO;2.

Belcher, S.E., Grant, A.L.M., Hanley, K.E., Fox-Kemper, B., Van Roeke, L., Sullivan, P.P., Large, W.G., Brown, A., Hines, A., Calvert, D., Rutgersson, A., Pettersson, H., Bidlot, J.-R., Janssen, P.A.E.M, and Polton, J.A. (2012). A global perspective on Langmuir turbulence in the ocean surface boundary layer. *Geophysical Research Letters*, 39(17). doi:10.1029/2012GL052932.

Bendat, J.S. and Piersol, A.G. (1986). *Random Data: Analysis and Measurement Procedures*, Second Edition, John Wiley & Sons, Inc., New York.

Bidlot, J.-R., Janssen, P., and Abdalla, S. (2007). A revised formulation of ocean wavedissipation and its model impact. *ECMFW Technical Report Memorandum*, 509 (January).

Björkqvist, J.-V., Tuomi, L., Pettersson, H., Fortelius, C., Tikka, K., and Kahma, K.K. (2014). The effect of boundary field accuracy on high-resolution coastal wave modelling. In: *Measuring and Modeling of Multi-Scale Interactions in the Marine Environment - IEEE/OES Baltic International Symposium 2014, BALTIC 2014*.

Björkqvist, J.-V., Lukas, I., Alari, V., van Vledder, G.Ph., Hulst, S., Pettersson, H., Behrens, A., and Männik, A. (2018). Comparing a 41-year model hindcast with decades of wave measurements from the Baltic Sea. *Ocean Engineering*, 152, pp. 57–71. doi: 10.1016/J.OCEANENG.2018.01.048.

Booij, N., Ris, R., and Holthuijsen, L.H. (1999). A third-generation wave model for coastal regions 1. Model description and validation. *Journal of Geophysical Research*, 104(C4), pp. 7649–7666. doi:10.1029/98jc02622.

BSBD (2013). Baltic Sea Hydrographic Commission, Baltic sea bathymetry database version 0.9.3. `http://data.bshc.pro/`.

Casas-Prat, M. and Holthuijsen, L.H. (2010). Short-term statistics of waves observed in deep water. *Journal of Geophysical Research: Oceans*, 115(C9). doi: 10.1029/2009JC005742.

Cavaleri, L. and Bertotti, L. (2004). Accuracy of the modelled wind and wave fields in enclosed seas. *Tellus*, 56A, pp. 167–175.

Cavaleri, L., Abdalla, S., Benetazzo, A., Bertotti, L., Bidlot, J.-R., Breivik, Ø., Carniel, S., Jensen, R.E., Portilla-Yandun, J., Rogers, W.E., Roland, A., Sanchez-Arcilla, A., Smith, J.M., Staneva, J., Toledo, Y., van Vledder, G.Ph., and van der Westhuysen, A.J. (2018). Wave modelling in coastal and inner seas. *Progress in Oceanography*, 167, pp. 164–233. doi:10.1016/j.pocean.2018.03.010.

Cieślikiewicz, W. and Paplińska-Swerpel, B. (2008). A 44-year hindcast of wind wave fields over the Baltic Sea. *Coastal Engineering*, 55(11), pp. 894–905. doi: 10.1016/j.coastaleng.2008.02.017.

Datawell, B. (2017). Datawell Waverider Reference Manual, March 2019, *Datawell BV*, `http://www.datawell.nl/Support/Documentation/Manuals.aspx`

Donelan, M.A., Drennan, W.M., and Magnusson, A.K. (1996). Nonstationary Analysis of the Directional Properties of Propagating Waves. *Journal of Physical Oceanography*, 26(9), pp. 1901–1914. doi:10.1175/1520-0485(1996)026¡1901:NAOTDP¿2.0.CO;2.

Donelan, M.A., Hamilton, J., and Hui, W.H. (1985). Directional Spectra of Wind-Generated Waves. *Philosophical Transactions of the Royal Society A: Mathematical, Physical and Engineering Sciences*, 315(1534), pp. 509–562. doi: 10.1098/rsta.1985.0054.

Donelan, M.A. and Pierson, W.J. (1983). The Sampling Variability of Estimates of Spectra of Wind-Generated Gravity Waves. *Journal of Geophysical Research*, 88(C7), pp. 4381–4392. doi:10.1029/JC088iC07p04381.

Drennan, W.M., Donelan, M.A., Madsen, N., Katsaros, K.B., Terray, E.A., and Flagg, C.N. (1994). Directional Wave Spectra from a Swath Ship at Sea. *Journal of Atmospheric and Oceanic Technology*, 11(4), pp. 1109–1116. doi:10.1175/1520-0426(1994)011¡1109:DWSFAS¿2.0.CO;2.

Eldeberky, Y. (1996). Nonlinear transformation of wave spectra in the nearshore. Ph.D. thesis, *Delft University of Technology*.

Erm, A., Alari, V., Lips, I., and Kask, J. (2011). Resuspension of sediment in a semi-sheltered bay due to wind waves and fast ferry wakes. *Boreal Environment Research*, 16(suppl. A), pp. 149–163.

Forristall, G.Z. (1978). On the statistical distribution of wave heights in a storm. *Journal of Geophysical Research*, 83(C5), pp. 2353–2358. doi:10.1029/JC083iC05p02353.

Forristall, G.Z. (1981). Measurements of a saturated range in ocean wave spectra. *Journal of Geophysical Research*, 86(C9), pp. 8075–8084. doi:10.1029/JC086iC09p08075.

Grossmann, A. and Morlet, J. (1984). Decomposition of Hardy functions into square integrable wavelets of constant shape. *SIAM Journal on Mathematical Analysis*, 15(5), pp. 723–736. doi:10.1137/0515056.

Guimarães, P.V. (2018). Sea surface and energy dissipation. Ph.D. thesis, *Loire Bretagne University*.

Gutiérrez-Loza, L., Ocampo-Torres, F.J., and García-Nava, H. (2018). The Effect of Breaking Waves on CO2 Air–Sea Fluxes in the Coastal Zone. *Boundary-Layer Meteorology*, 168(2), pp. 343–360. doi:10.1007/s10546-018-0342-x.

Hara, T. and Karachintsev, A.V. (2003). Observation of Nonlinear Effects in Ocean Surface Wave Frequency Spectra. *Journal of Physical Oceanography*, 33(2), pp. 422–430. doi:10.1175/1520-0485(2003)033¡0422:OONEIO¿2.0.CO;2.

Hasselmann, K. (1962). On the non-linear energy transfer in a gravity-wave spectrum Part 1. General theory. *Journal of Fluid Mechanics*, 12(4), pp. 481–500. doi: 10.1017/S0022112062000373.

Hasselmann, K. (1974). On the spectral dissipation of ocean waves due to white capping. *Boundary-Layer Meteorology*, 6(1-2), pp. 107–127. doi:10.1007/BF00232479.

Hasselmann, K., Barnett, T.P., Bouws, E., Carlson, H., Cartwright, D.E., Enke, K., Ewing, J.A., Gienapp, H., Hasselmann, D.E., Kruseman, P., Meerburg, A., Muller, P., Olbers, D.J., Richter, K., Sell, W., and Walden, H. (1973). Measurements of Wind-Wave Growth and Swell Decay during the Joint North Sea Wave Project (JONSWAP). *Ergnzungsheft zur Deutschen Hydrographischen Zeitschrift*, A(12), pp. 1–95.

Hasselmann, K., Sell, W., Ross, D.B., Müller, P., Hasselmann, K., Sell, W., Ross, D.B., and Müller, P. (1976). A Parametric Wave Prediction Model. *Journal of Physical Oceanography*, 6(2), pp. 200–228. doi:10.1175/1520-0485(1976)006¡0200:APWPM¿2.0.CO;2.

Hasselmann, S., Hasselmann, K., Allender, J.H., Barnett, T.P., Hasselmann, S., Hasselmann, K., Allender, J.H., and Barnett, T.P. (1985). Computations and Parameterizations of the Nonlinear Energy Transfer in a Gravity-Wave Specturm. Part II: Parameterizations of the Nonlinear Energy Transfer for Application in Wave Models. *Journal of Physical Oceanography*, 15(11), pp. 1378–1391. doi:10.1175/1520-0485(1985)015¡1378:CAPOTN¿2.0.CO;2.

Hayashi, Y. (1982). Space-time spectral analysis and its applications to atmospheric waves. *Journal of the Meteorological Society of Japan*. Ser. II 60(1), pp. 156–171.

HIRLAM-B (2018). HIRLAM system documentation. `http://hirlam.org`.

Högström, U., Smedman, A., Sahlée, E., Drennan, W.M., Kahma, K.K., Pettersson, H., and Zhang, F. (2009). The Atmospheric Boundary Layer during Swell: A Field Study and Interpretation of the Turbulent Kinetic Energy Budget for High Wave Ages. *Journal of the Atmospheric Sciences*, 66(9), pp. 2764–2779. doi:10.1175/2009JAS2973.1.

Holthuijsen, L.H. (1983). Observations of the Directional Distribution of Ocean-Wave Energy in Fetch-Limited Conditions. *Journal of Physical Oceanography*, 13(2), pp. 191–207. doi:10.1175/1520-0485(1983)013¡0191:OOTDDO¿2.0.CO;2.

Huang, C.J. and Qiao, F. (2010). Wave-turbulence interaction and its induced mixing in the upper ocean. *Journal of Geophysical Research: Oceans*, 115(C4), pp. 1–12. doi: 10.1029/2009JC005853.

Janssen, P. (1991). Quasi-linear Theory of Wind-Wave Generation Applied to Wave Forecasting. *Journal of Physical Oceanography*, 21(11), pp. 1631–1642. doi:10.1175/1520-0485(1991)021¡1631:QLTOWW¿2.0.CO;2.

Janssen, P. (2009). On some consequences of the canonical transformation in the Hamiltonian theory of water waves. *Journal of Fluid Mechanics*, 637, pp. 1–44. doi: 10.1017/S0022112009008131.

Jönsson, A., Broman, B., and Rahm, L. (2003). Variations in the Baltic Sea wave fields. *Ocean Engineering*, 30(1), pp. 107–126. doi:10.1016/S0029-8018(01)00103-2.

Kahma, K.K. (1979). On a two-peak structure in steady-state fetch-limited wave spectra. Licentiate thesis in Geophysics, *University of Helsinki*.

Kahma, K.K. (1981). A Study of the Growth of the Wave Spectrum with Fetch. *Journal of Physical Oceanography*, 11(11), pp. 1503–1515. doi:10.1175/1520-0485(1981)011¡1503:ASOTGO¿2.0.CO;2.

Kahma, K.K. (1986). On prediction of the fetch-limited wave spectrum in steady wind. *Finnish Marine Research*, (253), pp. 53–78.

Kahma, K.K. and Calkoen, C.J. (1992). Reconciling Discrepancies in the Observed Growth of Wind-generated Waves. *Journal of Physical Oceanography*, 22(12), pp. 1389–1405. doi:10.1175/1520-0485(1992)022¡1389:RDITOG¿2.0.CO;2.

Kahma, K.K., Donelan, M.A., Drennan, W.M., and Terray, E.A. (2016a). Evidence of Energy and Momentum Flux from Swell to Wind. *Journal of Physical Oceanography*, 46(7), pp. 2143–2156. doi:10.1175/JPO-D-15-0213.1.

Kahma, K.K. and Pettersson, H. (1994). Wave growth in a narrow fetch geometry. *The Global Atmosphere and Ocean System*, 2, pp. 253–263.

Kahma, K.K., Pettersson, H., and Tuomi, L. (2003). Scatter Diagram Wave Statistics from the Northern Baltic Sea. *MERI – Report Series of the Finnish Institute of Marine Research*, 49, pp. 15–32.

Kahma, K.K., Björkqvist, J.-V., Johansson, M.M., Jokinen, H., Leijala, U., Särkkä, J., Tikka, K., and Tuomi, L. (2016b). *Turvalliset rakentamiskorkeudet Helsingin rannoilla 2020, 2050 ja 2100*. Technical report. 96, City of Helsinki, Real Estate Department, Geotechnical Division.

Kaitaranta, J., Niemistö, J., Buhvestova, O., and Nurminen, L. (2013). Quantifying sediment resuspension and internal phosphorus loading in shallow near-shore areas in the Gulf of Finland. *Boreal Environment Research*, 18(6), pp. 473–487.

Kenyon, K.E. (1969). Stokes drift for random gravity waves. *Journal of Geophysical Research*, 74(28), pp. 6991–6994. doi:10.1029/JC074i028p06991.

Kitaigorodskii, S.A. (1962). Applications of the theory of similarity to the analysis of wind generated wave motion as stochastic process. *American Geophysical Union of the National Academy of Sciences*, pp. 73–80.

Kitaigorodskii, S.A. (1983). On the Theory of the Equilibrium Range in the Spectrum of Wind-Generated Gravity Waves. *Journal of Physical Oceanography*, 13(5), pp. 816–827. doi:10.1175/1520-0485(1983)013¡0816:OTTOTE¿2.0.CO;2.

Kitaigorodskii, S.A., Krasitskii, V.P., and Zaslavskii, M.M. (1975). On Phillips' Theory of Equilibrium Range in the Spectra of Wind-Generated Gravity Waves. *Journal of Physical Oceanography*, 5(3), pp. 410–420. doi:10.1175/1520-0485(1975)005¡0410:OPTOER¿2.0.CO;2.

Komen, G.J., Hasselmann, K., Hasselmann, K., Komen, G.J., Hasselmann, K., and Hasselmann, K. (1984). On the Existence of a Fully Developed Wind-Sea Spectrum. *Journal of Physical Oceanography*, 14(8), pp. 1271–1285. doi:10.1175/1520-0485(1984)014¡1271:OTEOAF¿2.0.CO;2.

Komen, G.J., Cavaleri, L., Donelan, M.A., K.Hasselmann, Hasselmann, S., and Janssen, P. (1994). *Dynamics and Modelling of Ocean Waves*. Cambridge University Press, Cambridge.

Laakso, L., Mikkonen, S., Drebs, A., Karjalainen, A., Pirinen, P., and Alenius, P. (2018). 100 Years of atmospheric and marine observations at the Finnish Utö Island in the Baltic Sea. *Ocean Science*, 14(4), pp. 617–632. doi:10.5194/os-14-617-2018.

Langmuir, I. (1938). Surface Motion of Water Induce by Wind. *Science*, 87(2250), pp. 119–123. doi:10.1126/science.87.2250.119.

Leckler, F., Ardhuin, F., Peureux, C., Benetazzo, A., Bergamasco, F., and Dulov, V. (2015). Analysis and Interpretation of Frequency–Wavenumber Spectra of Young Wind Waves. *Journal of Physical Oceanography*, 45(10), pp. 2484–2496. doi:10.1175/JPO-D-14-0237.1.

Leijala, U., Björkqvist, J.-V., Johansson, M.M., Pellikka, H., Laakso, L., and Kahma, K.K. (2018). Combining probability distributions of sea level variations and wave run-up to evaluate coastal flooding risks. *Natural Hazards and Earth System Sciences*, 18, pp. 2785–2799. doi:10.5194/nhess-18-2785-2018.

Lenain, L. and Melville, W.K. (2017). Measurements of the directional spectrum across the equilibrium-saturation ranges of wind-generated surface waves. *Journal of Physical Oceanography*, 47(8), pp. 2123–2138. doi:10.1175/JPO-D-17-0017.1.

Ponce de León, S. and Guedes Soares, C. (2005). On the sheltering effect of islands in ocean wave models. *Journal of Geophysical Research: Oceans*, 110(C9). doi: 10.1029/2004JC002682.

Ponce de León, S. and Guedes Soares, C. (2010). The sheltering effect of the Balearic Islands in the hindcast wave field. *Ocean Engineering*, 37(7), pp. 603–610. doi: 10.1016/j.oceaneng.2010.01.011.

Li, J.G. (2011). Global Transport on a Spherical Multiple-Cell Grid. *Monthly Weather Review*, 139(5), pp. 1536–1555. doi:10.1175/2010mwr3196.1.

Liu, Q., Rogers, W.E., Babanin, A.V., Young, I.R., Romero, L., Zieger, S., Qiao, F., and Guan, C. (2019). Observation-Based Source Terms in the Third-Generation Wave Model WAVEWATCH III: Updates and Verification. *Journal of Physical Oceanography*, 49(2), pp. 489–517. doi:10.1175/jpo-d-18-0137.1.

Longuet-Higgins, M.S. (1952). On the Statistical Distribution of the Heights of Sea Waves. *Journal of Marine Research*, 11(3), pp. 245–266.

Longuet-Higgins, M.S. (1970). Longshore currents generated by obliquely incident sea waves, 1. *Journal of Geophysical Research*, 75(33), pp. 6790–6801. doi: 10.1029/jc075i033p06790.

Longuet-Higgins, M.S. (1980). On the distribution of the heights of sea waves: Some effects of nonlinearity and finite band width. *Journal of Geophysical Research*, 85(C3), p. 1519. doi:10.1029/JC085iC03p01519.

Mazarakis, N., Kotroni, V., Lagouvardos, K., and Bertotti, L. (2012). High-resolution wave model validation over the Greek maritime areas. *Natural Hazards and Earth System Sciences*, 12(11), pp. 3433–3440. doi:10.5194/nhess-12-3433-2012.

Meyer, Y. (1989). Orthonormal Wavelets. In: Combes Jean-Michel, , Grossmann, A., Philippe, and Tchamitchian, eds, *Wavelets*, pp. 21–37. Berlin, Heidelberg: Springer Berlin Heidelberg.

Monbaliu, J., Padilla-Hernández, R., Hagreaves, J.C., Albiach, J.C.C., Luo, W., Sclavo, M., and Günter, H. (2000). The spectral wave model, WAM, adapted for applications with high spatial resolution. *Coastal Engineering*, 41, pp. 41–62.

Nielsen, P. (1988). Three simple models of wave sediment transport. *Coastal Engineering*, 12(1), pp. 43–62. doi:10.1016/0378-3839(88)90014-2.

Perrie, W., Tang, C.L., Hu, Y., and DeTracy, B.M. (2003). The Impact of Waves on Surface Currents. *Journal of Physical Oceanography*, 33(10), pp. 2126–2140. doi: 10.1175/1520-0485(2003)033¡2126:TIOWOS¿2.0.CO;2.

Perrie, W., Toulany, B., Roland, A., Dutour-Sikiric, M., Chen, C., Beardsley, R.C., Qi, J., Hu, Y., Casey, M., and Shen, H. (2017). Modeling North Atlantic Nor'easters with Modern Wave Forecast Models. *Journal of Geophysical Research: Oceans*, 123, pp. 533–557. doi:10.1002/2017JC012868.

Pettersson, H. (2004). Wave growth in a narrow bay. Ph.D. thesis, *University of Helsinki*.

Pettersson, H. and Kahma, K.K. (2005). Directional measurements of wave growth in a short and narrow fetch geometry. *Journal of Atmospheric and Ocean Science*, 10(1), pp. 15–29. doi:10.1080/17417530500062853.

Pettersson, H., Kahma, K.K., and Tuomi, L. (2010). Wave Directions in a Narrow Bay. *Journal of Physical Oceanography*, 40(1), pp. 155–169. doi:10.1175/2009JPO4220.1.

Pettersson, H., Lindow, H., and Brüning, T. (2013). *Wave climate in the Baltic Sea 2012*, HELCOM, Baltic Sea Environment Fact Sheet 2018.

Phillips, O.M. (1958). The equilibrium range in the spectrum of wind-generated waves. *Journal of Fluid Mechanics*, 4(4), pp. 426–434. doi:10.1017/S0022112058000550.

Phillips, O.M. (1985). Spectral and statistical properties of the equilibrium range in wind-generated gravity waves. *Journal of Fluid Mechanics*, 156, pp. 505–531. doi: 10.1017/S0022112085002221.

Qiao, F., Yuan, Y., Yang, Y., Zheng, Q., Xia, C., and Ma, J. (2004). Wave-induced mixing in the upper ocean: Distribution and application to a global ocean circulation model. *Geophysical Research Letters*, 31(L11303), pp. 1–4. doi:10.1029/2004GL019824.

Randel, W.J. and Held, I.M. (1991). Phase speed spectra of transient eddy fluxes and critical layer absorption. *Journal of the Atmospheric Sciences*, 48(5), pp. 688–697.

Resio, D., Long, C.E., and Vincent, C.L. (2004). Equilibrium-range constant in wind-generated wave spectra. *Journal of Geophysical Research*, 109(C01018), pp. 1–14. doi: 10.1029/2003JC001788.

Resio, D. and Perrie, W. (1989). Implication of an f^{-4} Equilibrium Range for Wind-Generated Waves. *Journal of Physical Oceanography*, 19(2), pp. 193–204. doi: 10.1175/1520-0485(1989)019¡0193:IOAERF¿2.0.CO;2.

Rinne, H., Kaskela, A., Downie, A.L., Tolvanen, H., von Numers, M., and Mattila, J. (2014). Predicting the occurrence of rocky reefs in a heterogeneous archipelago area with limited data. *Estuarine, Coastal and Shelf Science*, 138, pp. 90–100. doi: 10.1016/j.ecss.2013.12.025.

Romero, L., Melville, W.K., Romero, L., and Melville, W.K. (2010). Airborne Observations of Fetch-Limited Waves in the Gulf of Tehuantepec. *Journal of Physical Oceanography*, 40(3), pp. 441–465. doi:10.1175/2009JPO4127.1.

Räämet, A. and Soomere, T. (2010). The wave climate and its seasonal variability in the northeastern Baltic Sea. *Estonian Journal of Earth Sciences*, 59(1), p. 100. doi: 10.3176/earth.2010.1.08.

Sahlée, E., Drennan, W.M., Potter, H., and Rebozo, M.A. (2012). Waves and air-sea fluxes from a drifting ASIS buoy during the Southern Ocean Gas Exchange experiment. *Journal of Geophysical Research: Oceans*, 117(C08003), pp. 1–12. doi: 10.1029/2012JC008032.

Seifert, F., Tauber, B., and Kayser, B. (2001). A high resolution spherical grid topography of the Baltic Sea – 2nd edition. In: *Baltic Sea Science Congress Stockholm 25-29. November 2001, Poster 147*.

Semedo, A., Saetra, Ø., Rutgersson, A., Kahma, K.K., and Pettersson, H. (2009). Wave-Induced Wind in the Marine Boundary Layer. *Journal of the Atmospheric Sciences*, 66(8), pp. 2256–2271. doi:10.1175/2009jas3018.1.

Soomere, T. and Keevallik, S. (2003). Directional and extreme wind properties in the Gulf of Finland Baltic. *Proceedings of the Estonian Academy of Sciences, Engineering*, 9(2), pp. 73–90.

Soukissian, T.H., Prospathopoulos, A.M., and Diamanti, C. (2004). Wind and Wave Data Analysis for the Aegean Sea - Preliminary Results. *Journal of Atmospheric & Ocean Science*, 8(2-3), pp. 163–189. doi:10.1080/1023673029000003525.

SPM (1984). Shore Protection Manual, Vol. I, *Dept. of the Army, Waterways Experiment Station, Corps of Engineers, Coastal Engineering Research Center,*.

Squire, V.A. (2007). Of ocean waves and sea-ice revisited. *Cold Regions Science and Technology*, 49(2), pp. 110–133. doi:10.1016/j.coldregions.2007.04.007.

Steele, M. (1992). Sea ice melting and floe geometry in a simple ice-ocean model. *Journal of Geophysical Research*, 97(C11), pp. 17729-17738.

Tamura, H., Drennan, W.M., Sahlée, E., and Graber, H.C. (2014). Spectral form and source term balance of short gravity wind waves. *Journal of Geophysical Research: Oceans*, 119(11), pp. 7406–7419. doi:10.1002/2014JC009869.

Terray, E., Donelan, M.A., Agrawal, Y., Drennan, W.M., Kahma, K.K., Williams, A., Hwang, P., and Kitaigorodskii, S.A. (1996). Estimates of Kinetic Energy Dissipation under Breaking Waves. *Journal of Physical Oceanography*, 26(5), pp. 792–807. doi: 10.1175/1520-0485(1996)026¡0792:EOKEDU¿2.0.CO;2.

Tisler, P., Gregow, E., Niemelä, S., and Savijärvi, H. (2007). Wind Field Prediction in Coastal Zone: Operational Mesoscale Model Evaluation and Simulations with Increased Horizontal Resolution. *Journal of Coastal Research*, 23(3), pp. 721–730. doi: 10.2112/05-0450.1.

Toba, Y. (1972). Local Balance in the Air–Sea Boundary Processes I. On the Growth Process of Wind Waves. *Journal of the Oceanographical Society of Japan*, 28, pp. 109–121. doi:10.1007/BF02109772.

Toba, Y. (1973). Local Balance in the Air–Sea Boundary Processes III. On the Spectrum of Wind Waves. *Journal of the Oceanographical Society of Japan*, 29, pp. 209–220. doi:10.1007/BF02109506.

Tolman, H.L. (2003). Treatment of unresolved islands and ice in wind wave models. *Ocean Modelling*, 5(3), pp. 219–231. doi:10.1016/S1463-5003(02)00040-9.

Tolman, H.L. and Chalikov, D.V. (1996). Source Terms in a Third-Generation Wind Wave Model. *Journal of Physical Oceanography*, 26, pp. 2497–2518.

Tolman, H.L., Balasubramaniyan, B., Burroughs, L.D., Chalikov, D.V., Chao, Y.Y., Chen, H.S., and Gerald, V.M. (2002). Development and Implementation of Wind-Generated Ocean Surface Wave Modelsat NCEP. *Weather and Forecasting*, 17(2), pp. 311–333. doi:10.1175/1520-0434(2002)017¡0311:DAIOWG¿2.0.CO;2.

Tuomi, L. and Björkqvist, J.-V. (2014). Wave forecasting in coastal archipelagos. In: *Measuring and Modeling of Multi-Scale Interactions in the Marine Environment - IEEE/OES Baltic International Symposium 2014, BALTIC 2014*.

Tuomi, L., Kahma, K.K., and Pettersson, H. (2011). Wave hindcast statistics in the seasonally ice-covered Baltic Sea. *Boreal Environment Research*, 16(6), pp. 451–472.

Tuomi, L., Pettersson, H., Fortelius, C., Tikka, K., Björkqvist, J.-V., and Kahma, K.K. (2014). Wave modelling in archipelagos. *Coastal Engineering*, 83, pp. 205–220.

Tuomi, L., Vähä-Piikkiö, O., Alenius, P., Björkqvist, J.-V., and Kahma, K.K. (2018). Surface Stokes drift in the Baltic Sea based on modelled wave spectra. *Ocean Dynamics*, 68(1), pp. 17–33. doi:10.1007/s10236-017-1115-7.

Vandever, J.P., Siegel, E.M., Brubaker, J.M., and Friedrichs, C.T. (2008). Influence of Spectral Width on Wave Height Parameter Estimates in Coastal Environments. *Journal of Waterway, Port, Coastal, and Ocean Engineering*, 134(3), pp. 187–194. doi: 10.1061/(ASCE)0733-950X(2008)134:3(187).

van Vledder, G.Ph. (2006). The WRT method for the computation of non-linear four-wave interactions in discrete spectral wave models. *Coastal Engineering*, 53(2-3), pp. 223–242. doi:10.1016/j.coastaleng.2005.10.011.

WAMDIG (1988). The WAM Model—A Third Generation Ocean Wave Prediction Model. *Journal of Physical Oceanography*, 18(12), pp. 1775–1810. doi:10.1175/1520-0485(1988)018¡1775:TWMTGO¿2.0.CO;2.

Wang, D.W. and Hwang, P. (2004). The Dispersion Relation of Short Wind Waves from Space–Time Wave Measurements. *Journal of Atmospheric and Oceanic Technology*, 21(12), pp. 1936–1945. doi:10.1175/JTECH-1669.1.

van der Westhuysen, A.J., Zijlema, M., and Battjes, J.A. (2007). Nonlinear saturation-based whitecapping dissipation in SWAN for deep and shallow water. *Coastal Engineering*, 54(2), pp. 151–170. doi:10.1016/j.coastaleng.2006.08.006.

Wu, J. (1982). Wind-stress coefficients over sea surface from breeze to hurricane. *Journal of Geophysical Research*, 87(C12), pp. 9704–9706. doi:10.1029/JC087iC12p09704.

Young, I.R. (1995). The determination of confidence limits associated with estimates of the spectral peak frequency. *Ocean Engineering*, 22(7), pp. 669–686. doi: 10.1016/0029-8018(95)00002-3.

Zieger, S., Babanin, A.V., Erick Rogers, W., and Young, I.R. (2015). Observation-based source terms in the third-generation wave model WAVEWATCH. *Ocean Modelling*, 96(1), pp. 2–25. doi:10.1016/j.ocemod.2015.07.014.